Geodynamics and Consequences of Lithospheric Removal
in the Sierra Nevada, California themed issue

Structure of the Sierra Nevada from receiver functions and implications for lithospheric foundering

Andrew M. Frassetto[1,2,*], George Zandt[2], Hersh Gilbert[3], Thomas J. Owens[4], and Craig H. Jones[5]
[1]*Department of Geography and Geology, University of Copenhagen, Øster Voldgade 10, 1350 Copenhagen K, Denmark*
[2]*Department of Geosciences, University of Arizona, Gould-Simpson Building #77, 1040 E 4th Street, Tucson, Arizona 85721, USA*
[3]*Department of Earth and Atmospheric Sciences, Purdue University, 550 Stadium Mall Drive, West Lafayette, Indiana 47907, USA*
[4]*Department of Earth and Ocean Sciences, University of South Carolina, 701 Sumter Street, EWS 617, Columbia, South Carolina 29208, USA*
[5]*Department of Geological Sciences, University of Colorado, Campus Box 399, 2200 Colorado Avenue, Boulder, Colorado 80309-0399, USA*

ABSTRACT

Receiver functions sampling the Sierra Nevada batholith and adjacent regions exhibit significant variations in the structure of the crust and upper mantle. Crustal Vp/Vs values are lower in the core of the batholith and higher in the northern Sierra Nevada, portions of the Basin and Range, and near young volcanic fields in the eastern Sierra Nevada and Owens Valley. P- to S-wave conversions from the Moho vary from high amplitude and shallow (>25% of the direct P-arrival amplitude, 25–35 km depth) along the eastern Sierra Nevada to low amplitude and deep (<10%, 45–55 km) beneath the western batholith. We propose that dense mafic-ultramafic residue has foundered in the east-central and southern Sierra Nevada but still resides beneath its western portion. The central and northern Sierra Nevada shows inherited, prebatholithic structure at the Moho that was not completely overprinted by emplacement of the massive end-stage batholith. Evidence for the development and/or loss of substantial residue in the northern Sierra Nevada is equivocal. The asymmetric structure of the lithosphere beneath the central Sierra, which we model using constraints from petrophysical analyses, suggests that foundering progresses from southeast to northwest. This process sharpens the seismic response of the Moho by removing its underlying lithospheric mantle and allows upwelling asthenosphere to replace the detached material. Deep crustal seismicity and recent volcanism observed to 38° N appear linked to this process and correlate spatially with the change in the character of the Moho, measurements of high crustal Vp/Vs, and presence of prominent negative conversions in the crust and uppermost mantle.

INTRODUCTION

Formation and eventual foundering of dense eclogitic residues or "arclogites" (Anderson, 2005) subjacent to Cordilleran arc volcanism play an important role in steering orogenesis and separating felsic continental crust from its basaltic source (Kay and Kay, 1991; Ducea, 2001; Kelemen et al., 2003; DeCelles et al., 2009). A type locality for this process, the Mesozoic-age southern Sierra Nevada batholith in western North America, retained its corresponding residual mass until relatively recently (e.g., Ducea, 2001). Following the demise of the subducting Farallon plate and development of a dextral transform that persists today (Dickinson and Snyder, 1979), gravitationally unstable lower crust and lithospheric mantle foundered beneath the southern Sierra Nevada and was replaced by buoyant asthenosphere (Ducea and Saleeby, 1996; Saleeby et al., 2003; Zandt et al., 2004). This process may explain why the region maintains a high elevation in the absence of tectonic compression (e.g., Wernicke et al., 1996). This study uses images of seismic structure to place new constraints on the geologic and tectonic state of the Sierra Nevada, gain insight into the foundering process, and explore evidence for ongoing foundering northward along the range.

Geologic and Tectonic Overview

The Sierra Nevada consist of westward sloping, fluvially and glacially incised igneous and metamorphic rocks, which extend east from the Great Valley and terminate along a 2–4+ km high crest bordered by normal faults that comprise the westernmost Basin and Range (Christensen, 1966; Bateman and Eaton, 1967; Bateman, 1988) (Fig. 1). The basement in the Sierra Nevada comprises ophiolitic assemblages and mélange sediments of Paleozoic-age and younger accreted to the continental margin and intruded by massive, mostly Mesozoic-age plutons during ocean-continent subduction (Dickinson, 1981; Saleeby, 1992; Ducea, 2001; Dickinson, 2008). A Jurassic-age accretion formed the heavily faulted Foothills Metamorphic Belt along the western edge of the central and northern Sierra Nevada (Schweickert et al., 1984). Granitoid plutons dominate the basement in the southern and central batholith but distribute more diffusely to the north (Bateman and Eaton, 1967; Bateman, 1988). The exposed batholith trends toward more mafic compositions in its western exposures (Bateman and Eaton, 1967), with widespread cumulates present to the axis of the Great Valley (Saleeby, 2007). Voluminous arc magmatism that created the majority of the batholith appears confined to distinct phases ca. 160–150 Ma and 100–85 Ma (Ducea, 2001).

Flat subduction during the Laramide extinguished the magmatic arc, dismembered the root of the batholith across the Mojave, and triggered exhumation of the southernmost Sierra Nevada; other parts of the range remained largely undisturbed until ca. 30 Ma (Malin et al., 1995; Saleeby, 2003; Chapman et al., 2010). The formation and northward migration of the Mendocino triple junction and development of the San Andreas fault halted subduction and opened a slab window beneath the region (Dickinson, 1979; Dickinson, 1981). Tectonic reconstructions (e.g., Atwater and Stock, 1998) show

*Present address: Incorporated Research Institutions for Seismology, 1200 New York Avenue, NW, Suite 800, Washington, D.C. 20005, USA; drrocks1982@gmail.com.

Geosphere; August 2011; v. 7; no. 4; p. 898–921; doi: 10.1130/GES00570.1; 20 figures; 3 tables.

that the southern edge of the subducting Juan de Fuca plate passed beneath the southern Sierra Nevada at 20–15 Ma, cleared the central Sierra Nevada by 5 Ma, and is currently positioned just north of Lake Tahoe in agreement with teleseismic tomography (e.g., Schmandt and Humphreys, 2010). A westward sweep of basaltic andesite and dacite magmas into the central and northern Sierra Nevada from ca. 20–15 Ma records the emergence of the ancestral Cascade arc between Yosemite National Park and Lake Tahoe (Busby et al., 2008; Cousens et al., 2008; Busby and Putirka, 2009). Basaltic magmas erupted through the southern and central Sierra Nevada and adjacent Basin and Range beginning in the Miocene (Manley et al., 2000). A Pliocene-age episode of potassic volcanism in the central and eastern Sierra Nevada indicates melting and remobilization of Precambrian mantle lithosphere and was followed by basaltic and bimodal eruptions across the eastern Sierra Nevada and Walker Lane (Manley et al., 2000; Farmer et al., 2002).

Evidence for Lithospheric Removal

Thermobarometry of xenoliths carried in magmas erupted since the Miocene reflects a distinct temporal evolution in the composition, density, temperature, and dimension of the lower crust and mantle lithosphere. Volcanism across the central Sierra Nevada at ca. 10–8 Ma produced xenoliths sampling a lithospheric column >100 km thick containing mafic granulite, garnet-clinopyroxenite, ultramafic websterite, and garnet-peridotite (Mukhopadhyay and Manton, 1994; Ducea and Saleeby, 1996). The crustally-derived xenoliths record eclogite facies conditions beginning at ~40 km depth, sample crustal material to as deep as 65–70 km and preserve residual assemblages consistent with extraction of felsic melts (Ducea and Saleeby, 1996, 1998a). Xenoliths from the Quaternary-age volcanic centers, located just east of the Miocene-age locations, sample only lherzolite and harzburgite from as shallow as 35 km depth. These record pressure-temperature (P-T) conditions of 1200 °C at 1–1.2 GPa, indicating that convective asthenosphere encroaches on the crust-mantle boundary beneath the eastern Sierra Nevada (Ducea and Saleeby, 1996). The garnet-rich residuum beneath the central Sierra Nevada equilibrated almost entirely during the Cretaceous (Ducea and Saleeby, 1998a). Due to the extremely high density (~3500 kg/m^3) of rock type, Ducea and Saleeby (1996, 1998b) suggest that foundering of this material allowed for an upwelling of asthenosphere and corresponding density reduction needed to elevate the range. Invading asthenosphere represents a potential trigger for the extension and volcanism occurring since the Pliocene in the eastern Sierra Nevada and western Basin and Range (Jones et al., 2004).

Many geophysical investigations (Jones et al., 1994; Fliedner et al., 1996; Ruppert et al., 1998; Jones and Phinney, 1998; Zandt et al., 2004) corroborate the lack of mantle lithosphere and isostatic crustal root beneath the southern Sierra Nevada. The predominantly granitoid crust is likely supported by a region of seismically slow, conductive, buoyant asthenosphere (Fliedner et al., 1996; Savage et al., 2003; Park, 2004). Tomographic and magnetotelluric images (Benz and Zandt, 1993; Jones et al., 1994; Boyd et al., 2004; Park, 2004; Yang and Forsyth, 2006; Reeg et al., 2008; Schmandt and Humphreys, 2010) beneath the southern Great Valley and western batholith reveal a cylindrical zone of fast, resistive material ranging from the base of the crust to nearly 250 km depth. This feature, commonly referred to as the "drip" or "Isabella anomaly" (Fig. 1), is interpreted as downwelling lithospheric mantle and eclogitic lower crust that foundered from the southern Sierra Nevada (Saleeby et al., 2003; Zandt et al., 2004) and produces subsidence beneath the southern Great Valley (Saleeby and Foster, 2004).

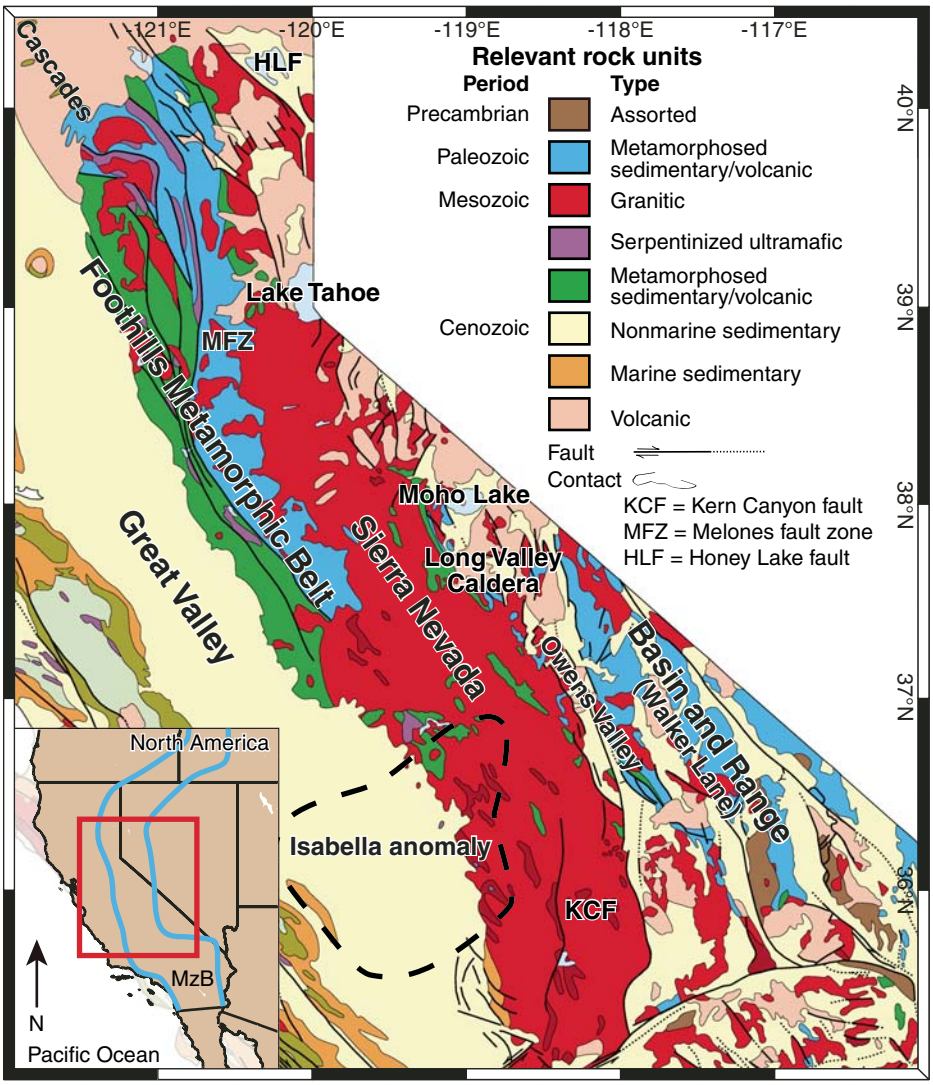

Figure 1. Simplified geologic map of the Sierra Nevada and vicinity (cf. Parrish, 2006). The inset map provides a frame of reference for the southwestern United States and outlines (blue) the approximate boundaries of Mesozoic-age batholith (MzB) (Barton and Hanson, 1989). Plutons (red) are generally associated with the Sierra Nevada batholith. The outlined Isabella anomaly at 125 km depth is from P-wave tomography (Schmandt and Humphreys, 2010).

Several groups contest the timing and magnitude of major elevation changes, if any, throughout the Sierra Nevada during the Cenozoic (cf. Cassel et al., 2009). Westward tilt observed in strata and preserved in faulting along the eastern escarpment suggests that the Sierra Nevada have risen by ~2 km over the past several million years (Huber, 1981; Unruh, 1991; Wakabayashi and Sawyer, 2001). Evidence for the lithospheric foundering coincides generally with the timing and location of this uplift, and has been invoked as a potential trigger (e.g., Jones et al., 2004).

Motivation for the Sierra Nevada EarthScope Project

The departure of arclogite from beneath southern Sierra Nevada is well constrained, but large-scale geophysical heterogeneities in the central and northern Sierra Nevada are evidence that the batholithic root may be more intact. Reduced heat-flow measurements transition from some of the lowest (~20 mW/m^2) in North America along the Great Valley to considerably higher (>60 mW/m^2) in the eastern Sierra Nevada and adjacent Walker Lane (Lachenbruch and Sass, 1977; Saltus and Lachenbruch, 1991; Blackwell and Richards, 2004). A similar trend is observed in Bouguer gravity, which drops ~200 mgal eastward to a regional low centered along the eastern Sierra Nevada (Oliver, 1977). Directionally dependent refractions from the Moho suggest that a complicated crust-mantle transition underlies the western Sierra Nevada (Jones, 1987; Savage et al., 1994).

Structural mapping with a densely sampled teleseismic converted wave field, using a focused data set, provides the opportunity to better characterize the crust and upper mantle throughout the entire Sierra Nevada. Understanding variations in the thickness of the crust, its internal structure, bulk composition, and relation to the underlying mantle places fundamental constraints on the presence or absence of batholithic residue and the potential consequences of foundering. In addition to using converted waves as a structural mapping tool and proxy for crustal Vp/Vs, we also calculate Vp/Vs using arrivals from local earthquakes and modal compositions from crustal xenoliths as additional comparative constraints.

TELESEISMIC DATA AND RECEIVER-FUNCTION ANALYSIS

Station and Event Selection

The Sierra Nevada EarthScope Project (SNEP) operated broadband seismometers in the central and northern Sierra Nevada from May 2005 through September 2007 (Gilbert et al., 2007) (Fig. 2). Our data set encompasses 90 SNEP stations and 76 additional three-component intermediate-period or broadband instruments from monitoring networks, USArray, and previous experiments (Jones and Phinney, 1998; Wilson et al., 2003; Zandt et al., 2004) that recorded between July 1993 and September 2007 (Table 1). Most stations are spaced ~20–25 km apart with the exception of 14 stations densely deployed through Yosemite National Park.

We consider events from great-circle–path distances of 25°–95° and 95°–180° for P and PP arrivals, respectively. To ensure a sufficient amount of data, we collect events with M >5 for temporary deployments, M >5.6 for USArray sites, and M >6 for permanent stations. Our event distribution shows good distance coverage but samples directions mostly associated with the circum-Pacific subduction zones (Fig. 3).

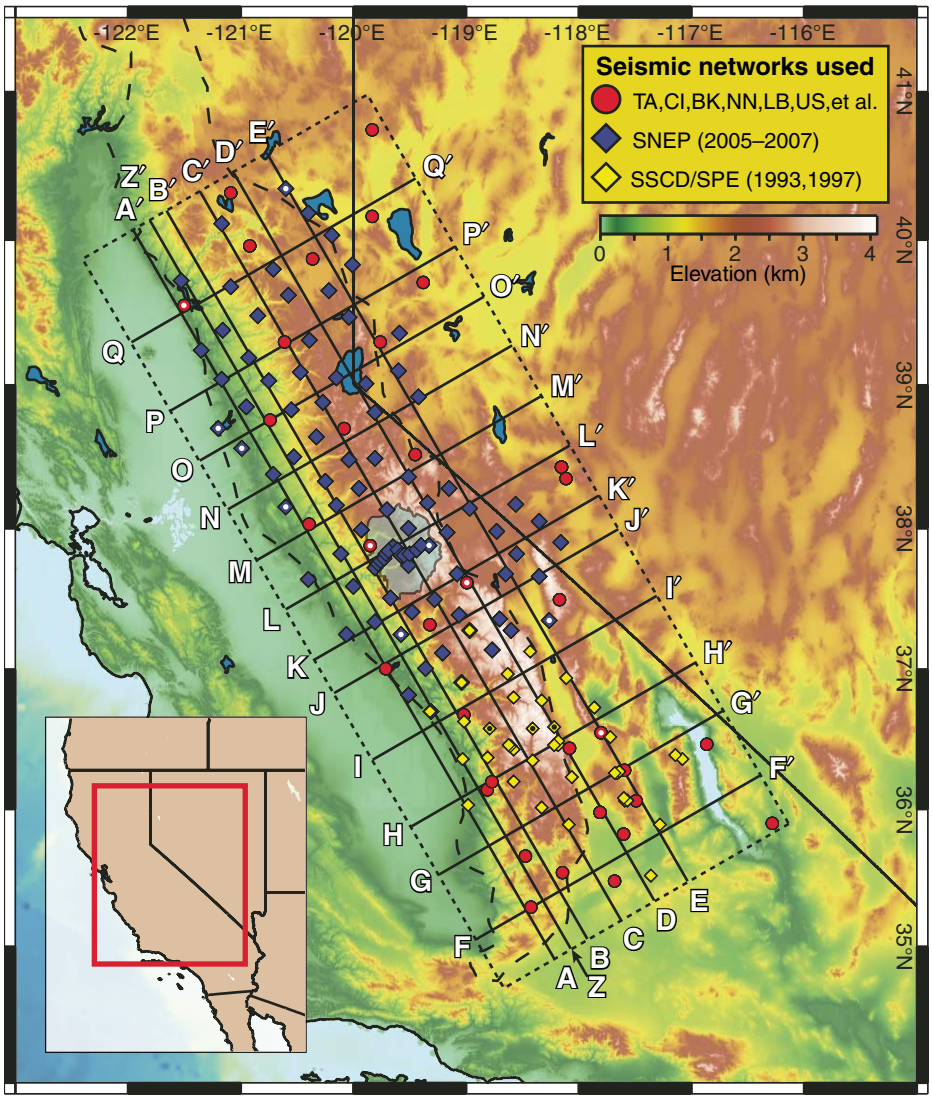

Figure 2. Broadband stations analyzed in this study. The dashed rectangle encloses the area studied as part of the Sierra Nevada EarthScope Project. Labeled lines represent transects of receiver functions (Figs. 11, 12, 15, 18, and 20). The outline of the Sierra Nevada batholith and Cascade volcanic arc is referenced in later figures. Yosemite National Park is highlighted blue. Stations that are presented individually are marked with dots (white—Figs. 4 and 5; black—Fig. 13). Network abbreviations: SSCD—Southern Sierra Continental Dynamics Project; SPE—Sierra Paradox Experiment; TA—USArray Transportable Array; CI—Caltech Regional Seismic Network; BK—Berkeley Digital Seismic Network; NN—Nevada Regional Network; LB—Leo Brady Network; US—United States National Seismic Network.

TABLE 1. STATIONS USED IN THIS STUDY

Station	Latitude	Longitude	Elevation	Number of receiver functions			Station	Latitude	Longitude	Elevation	Number of receiver functions		
				a = 1	*a* = 2.5	*a* = 5					*a* = 1	*a* = 2.5	*a* = 5
ARC2	36.01	−118.33	2597	15	17	15	SNP43	37.41	−119.48	2274	102	112	108
BEK[90]	39.87	−120.36	1743	202	235	221	SNP44	37.5	−119.28	2070	73	78	79
BGR	36.63	−119.02	954	23	27	28	SNP45	37.68	−119.08	2571	34	42	45
BPC	37.13	−118.43	2370	17	17	11	SNP47	37.98	−118.73	2074	71	77	73
BRR	36.91	−119.04	1259	22	27	28	SNP48	38.17	−118.56	1838	67	76	78
BVC	36.73	−117.86	483	9	11	11	SNP51	37.25	−120.06	250	94	131	135
CCC	36.58	−118.79	1560	11	13	13	SNP52	37.34	−119.81	341	63	78	82
CCC	35.52	−117.36	670	78	64	77	SNP53	37.51	−119.67	1459	60	75	83
CGO	36.55	−117.8	2795	152	180	166	SNP54	37.74	−119.51	1868	54	75	77
CHP	35.89	−118.09	2426	5	7	8	SNP55	37.88	−119.33	2693	121	139	146
CLC	35.82	−117.6	775	193	220	225	SNP56	37.97	−119.17	2944	40	50	51
CMB[90]	38.03	−120.39	697	484	398	325	SNP57	38.14	−118.97	2090	65	61	61
CPR	36.8	−118.58	1603	22	23	23	SNP62	37.59	−120	651	51	60	59
CWC[85]	36.44	−118.08	1595	244	300	301	SNP63	37.72	−119.81	1906	135	163	172
DAC[85]	36.28	−117.59	1813	183	232	233	SNP64	37.87	−119.65	2423	144	169	181
DP00	36.26	−117.66	1725	19	25	28	SNP65	38	−119.51	2911	99	125	129
DPE4	36.27	−117.64	1684	2	2	2	SNP66	38.18	−119.34	2429	47	38	35
DPW4	36.26	−117.68	1669	2	2	2	SNP67	38.28	−119.15	2277	64	83	83
FLL	37.28	−118.97	2237	20	23	25	SNP71	37.64	−120.4	157	75	88	95
FUR	36.47	−116.86	−37	191	217	188	SNP73	37.82	−120.11	982	73	90	100
HELL	36.68	−119.02	1145	171	207	222	SNP74	37.99	−119.93	1684	121	153	162
HFEB	36.36	−117.08	1650	25	30	30	SNP75	38.13	−119.7	2665	73	88	100
HFN7	36.39	−117.14	1516	10	10	12	SNP76	38.36	−119.51	2106	56	67	54
HM00	36.46	−118.18	3155	5	5	5	SNP84	38.16	−120.15	1610	104	123	125
HMN5	36.49	−118.18	3133	7	9	9	SNP85	38.28	−119.95	2003	91	120	127
HMW5	36.46	−118.22	3459	7	7	8	SNP86	38.49	−119.81	2632	141	166	184
HVY	36.7	−119.32	193	12	16	17	SNP93	38.15	−120.6	402	112	136	139
ISA[85]	35.66	−118.47	873	265	300	311	SNP95	38.33	−120.25	1754	100	118	124
JRC	35.98	−117.81	1452	75	90	88	SNP96	38.48	−120.04	2243	109	131	133
JRC2	35.98	−117.81	1469	110	138	126	SNP97	38.81	−119.81	1770	73	30	13
JUN	36.58	−118.41	2471	16	18	21	SNP98	38.92	−119.42	1521	39	35	28
KCC[85]	37.32	−119.32	888	225	253	255	SNPA3	38.38	−120.71	578	111	134	135
LAVA	38.76	−120.74	828	176	197	201	SNPA4	38.5	−120.54	1146	80	84	77
LBT00	36.06	−117.59	1810	2	2	2	SNPA5	38.64	−120.33	1744	99	130	136
LBTE5	36.06	−117.57	1805	10	14	13	SNPA7	39.01	−119.89	2350	82	87	82
LBTN5	36.08	−117.6	1724	4	6	6	SNPA8	39.1	−119.6	2004	60	60	63
LMC	36.36	−119.03	211	15	17	18	SNPB3	38.56	−120.99	245	95	109	120
LRL	35.48	−117.68	1340	191	245	257	SNPB5	38.83	−120.55	1413	47	50	50
MK00	36.45	−118.6	2437	4	5	6	SNPB6	38.88	−120.27	2230	61	72	70
MKS5	36.43	−118.58	2548	2	1	1	SNPB7	39.05	−120.15	2021	53	34	15
MKW3	36.45	−118.61	2358	0	1	1	SNPB9	39.36	−119.59	1855	92	82	66
MKW5	36.46	−118.62	2228	5	6	7	SNPC3	38.7	−121.2	76	108	140	146
MNV[85]	38.43	−118.15	1524	281	307	304	SNPC4	38.85	−120.95	516	78	83	84
MPM[90]	36.06	−117.49	1839	211	236	197	SNPC5	39.03	−120.75	1006	88	105	102
N06A	40.75	−119.83	1341	98	118	124	SNPC6	39.09	−120.47	1887	96	100	85
NV31	38.43	−118.15	1585	180	221	217	SNPC7	39.31	−120.39	2281	102	123	132
O04C	40.32	−121.09	1513	150	172	141	SNPC8	39.47	−120.04	2562	51	66	37
O05C	39.96	−120.92	1032	140	69	48	SNPD4	39.04	−121.17	402	94	92	96
O06A	40.17	−119.83	1229	28	37	37	SNPD5	39.19	−120.93	792	92	93	92
OMM	37.62	−118.99	2750	42	50	45	SNPD7	39.62	−120.58	1690	70	80	81
ORV[95]	39.55	−121.5	335	267	271	259	SNPD8	39.65	−120.22	1546	101	136	128
OVY	36.78	−118.33	2704	16	17	16	SNPD9	39.83	−120.01	1608	55	45	29
P05C	39.3	−120.61	1757	172	208	213	SNPE4	39.24	−121.35	88	107	121	125
PAH[85]	39.71	−119.38	1500	197	250	244	SNPE5	39.38	−121.16	945	87	115	120
PDC	36.03	−118.98	167	19	21	22	SNPE6	39.48	−120.85	1479	86	98	97
R05C	38.7	−120.08	2366	151	179	186	SNPE7	39.8	−120.71	1537	56	58	55
R06C	38.52	−119.45	1698	131	145	121	SNPE9	40.03	−120.19	1797	100	128	115
R08A	38.35	−118.11	1420	97	81	56	SNPF6	39.68	−121.09	1535	96	103	92
S06C	37.88	−119.85	1377	149	178	184	SNPF9	40.18	−120.4	1331	78	111	111
S08C	37.5	−118.17	3087	159	193	202	SNPG5	39.72	−121.53	652	82	95	95
SFK	36.37	−118.81	812	8	9	9	SNPG7	40.11	−121.17	1591	31	35	31
SFT	36.23	−118.06	1753	15	17	15	SNPG9	40.35	−120.6	1332	87	126	147
SHO	35.9	−116.28	451	221	174	112	SPG	36.14	−118.81	314	114	138	135
SLA[90]	35.89	−117.28	1174	258	282	216	SPG2	36.2	−118.77	627	57	62	64
SLC	36.52	−117.72	1918	17	19	19	SRF	36.94	−118.11	2148	20	24	23
SMD	36.97	−118.63	1807	19	24	26	T06C	37.01	−119.71	216	173	211	219
SNP11	36.7	−119.31	171	65	89	99	TEH	35.29	−118.42	846	163	177	181
SNP12	36.91	−119.04	1259	97	125	124	TWR2	36.35	−118.41	1946	15	15	17
SNP14	37.14	−118.77	3072	106	116	117	WBS	35.54	−118.14	1927	138	175	159
SNP15	37.28	−118.6	2434	35	23	13	WCN[90]	39.3	−119.76	1500	263	302	211
SNP16	37.35	−118.26	1898	61	72	67	WHP	36.59	−118.22	2388	16	18	17
SNP21	36.82	−119.51	229	55	71	74	WMD	36.2	−118.58	2592	18	17	18
SNP22	37.01	−119.36	1207	67	83	91	YOS01	37.75	−119.78	1866	45	48	47
SNP23	37.12	−119.21	2087	78	90	93	YOS02	37.77	−119.76	2116	38	39	40
SNP24	37.28	−118.97	2237	35	39	40	YOS03	37.79	−119.73	2078	41	39	40
SNP25	37.36	−118.7	2466	45	48	46	YOS04	37.82	−119.71	2210	47	49	51
SNP27	37.66	−118.35	1739	56	58	38	YOS05	37.84	−119.69	2385	43	47	51
SNP28	37.9	−118.16	1641	55	41	33	YOS06	37.85	−119.61	2507	40	46	49
SNP34	37.39	−119.06	2401	87	107	115	YOS07	37.81	−119.58	2495	40	43	48
SNP36	37.68	−118.65	2457	56	72	53	YOS08	37.81	−119.55	2493	36	38	36
SNP37	37.82	−118.55	1939	65	93	94	YOS09	37.82	−119.5	2575	35	43	46
SNP38	38.05	−118.35	2063	70	83	83	YOS10	37.85	−119.44	2576	36	41	41
SNP42	37.25	−119.58	942	54	64	67	YOS11	37.88	−119.4	2624	31	33	34

Note: Coordinates are listed in degrees and meters. A variance reduction cutoff of 80% is used when selecting receiver functions except where otherwise noted. Total counts are *a* = 1: 13829; *a* = 2.5: 15646; *a* = 5: 15208.

We omit events with signal-to-noise ratio <2 for the P arrival and its coda, leaving 69520 P and PP seismograms representing unique event-station pairs.

Receiver-Function Processing

Receiver functions (e.g., Langston, 1979) measure the seismic impedance structure of the crust and upper mantle. We bandpass seismograms from 0.15–5 Hz to isolate interference from the microseism and cultural noise, rotate into the R-T-Z coordinate system, and calculate receiver functions using iterative, time-domain deconvolution (Ligorría and Ammon, 1999). In general, deconvolution removes source and instrument effects to preserve P-SV conversions (hereafter called Ps) generated by an upgoing, teleseismic P wave interacting with subhorizontal structure beneath a seismometer. Iterative deconvolution, which constructs a time series of Gaussian spikes using a cross-correlation of the vertical and radial component seismograms, avoids the lesser elements of traditional spectral division such as the need for regularization and appearance of frequency side-lobes due to missing spectra. For each deconvolution, we iterate 400 times or until the misfit of the calculated receiver function is reduced by less than 0.001. We use Gaussian width factors (termed *"a"* values) of 1, 2.5, and 5 during deconvolution, corresponding to low-pass filters with corner frequencies of 0.5, 1.2, and 2.4 Hz, which are sensitive to structures thicker than ~2.0, 0.8, and 0.4 km for the crust and upper mantle. Additional resources on the theoretical development and practical considerations of receiver functions are plentiful (Langston, 1979; Owens and Zandt, 1985; Cassidy, 1992; Gurrola et al., 1994; Ligorría and Ammon, 1999; Julià, 2007; Frassetto et al., 2010).

Receiver functions are normalized so that the P arrival has unit amplitude equal to 1 near 0 seconds lag time, increasing the amplitudes of subsequent arrivals, an effect which is addressed in stacking. We retain receiver functions with variance reductions ≥80% (Ligorría and Ammon, 1999) that exhibit the expected response for a normalized radial receiver function: the maximum amplitude equals 1 near 0 seconds lag time, negative amplitudes do not exceed −1, and the P arrival is not preceded by a negative trough or significant delay. Additional spurious data were removed after visual inspection, and in several cases entire stations were omitted due to the presence of resonant signal from shallowly sourced reverberations. To avoid biasing stacked data, we also eliminate receiver functions with 80%–95% variance reduction at several permanent stations with substantially more data than adjacent temporarily deployed stations (Table 1).

We utilize common–conversion-point (CCP) stacking (Dueker and Sheehan, 1997; Gilbert et al., 2003) to migrate receiver functions into a three-dimensional structural volume. This method weights and averages the amplitudes of separate receiver functions that intersect a similar region of the subsurface. Our approach generally obeys the steps described by Dueker and Sheehan (1998) and Gilbert et al. (2003). Here we rotate the stacking bins to 30° counterclockwise from north to follow the strike of the Sierra Nevada (Fig. 2). To account for the +4 km of relief across the region, we remove the contribution from topography. We combine the SNEP teleseismic P-wave tomography (Reeg et al., 2008) and our Vp/Vs analyses to create a 3-D wave-speed model for pre-stack depth migration. The P–wave-speed (Vp) model is calculated from the observed deviation in percentage from IASP91 (Kennett and Engdahl, 1991) for the 20 km and 70 km depth slices. The S–wave-speed (Vs) model is calculated from estimated crustal Vp/Vs to 60 km depth and Vp/Vs of 1.85 below that.

Receiver functions are corrected for move out, converted to depth, and back-projected along their incoming ray paths into gridded bins spaced at 15 km intervals with each bin having a horizontal radius of 20 km and vertical thickness of ½ km. Sharing data across bins closes gaps in ray coverage caused by nonuniform spacing and enhances the lateral coherency of conversions. Bins containing less than ten receiver functions are discarded. Each trace is multiplied by i_r/i, where i_r is a depth-invariant reference angle (20°) and i is the incidence angle calculated from P slowness. This term rescales normalized amplitudes as a function of distance. Finally, we stack with a phase-weighting filter (Schimmel and Paulssen, 1997) to suppress various forms of signal-generated noise often prevalent in complicated geologic environments. We present this technique and its application to SNEP in a separate study (Frassetto et al., 2010).

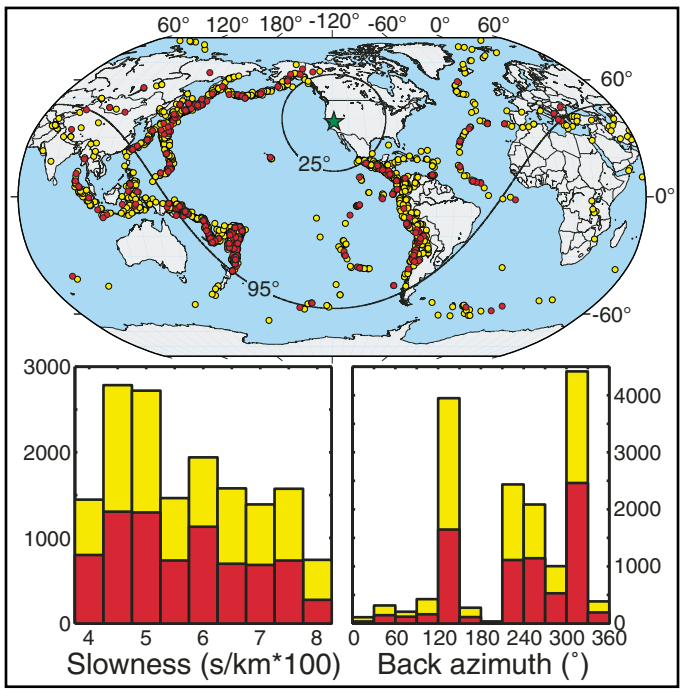

Figure 3. Events recorded by all stations (yellow) and only Sierra Nevada EarthScope Project (red). The map shows distance ranges of events producing P (distances of 25–95°) and PP arrivals (95–180°). The green triangle represents the center of the study area.

Sources and Estimates of Uncertainties

Identifying sources of uncertainty in the CCP stacks adds constraints to subsequent interpretations. Examining uncertainties in the depth and amplitude of the Moho Ps is especially important in this study. The average bin for a = 2.5 at 40 km depth stacks ~106 receiver functions with a mean variance reduction of 90.5%, demonstrating robust deconvolution and ray coverage. We stack 200 times using bootstrapping (Efron and Tibshirani, 1986) to reduce the effects of spurious noise. We automatically

select the largest positive arrival from 20 to 70 km depth and refine these picks for each bin. We reject one-third of picks lying farthest from the median depth, compute the standard deviation (σ) of the remaining values, and omit estimates with σ >5 km. Despite having the lowest practical depth resolution, for a = 1 the mean uncertainties for depth and conversion amplitude are only 1 km and 1.3%, respectively, with the largest at any bin being 2.5 km and 5.7%. It therefore appears that variance due solely to noise is small for SNEP.

Considering uncertainties in migrated interface depth introduced by the Vp and Vs assumptions is also important and has been examined previously (Calkins et al., 2010; Frassetto et al., 2010). For 55 km thick crust (Vp = 6.6 km/s, Vp/Vs = 1.76), a significant range in Vp/Vs (±2.5%) would change the migrated depth by <±4 km. Migrated receiver functions are less sensitive to the Vp model, and varying it similarly adjusts depth by only ±1.4 km. Subsequently calculated crustal Vp/Vs values show mean standard deviation of 0.8% for SNEP, translating to ±1.2 km of variation. Uncertainties associated with the P-wave tomography are <0.3%, which translates to ±0.2 km (Reeg et al., 2008). Uncertainties for shallower structures will be proportionally smaller, except perhaps in the upper crust where Vp and Vs are probably overestimated. Considering these dependencies, we can expect a combined potential uncertainty of < ±2.6 km in depth for the Moho throughout the Sierra Nevada.

OBSERVATIONS

Individual Stations

The SNEP data set is generally excellent quality; many stations operated for over a year and produced >100 usable receiver functions (Table 1). The array is embedded within a backbone of stations with substantially longer deployments. We removed several stations that

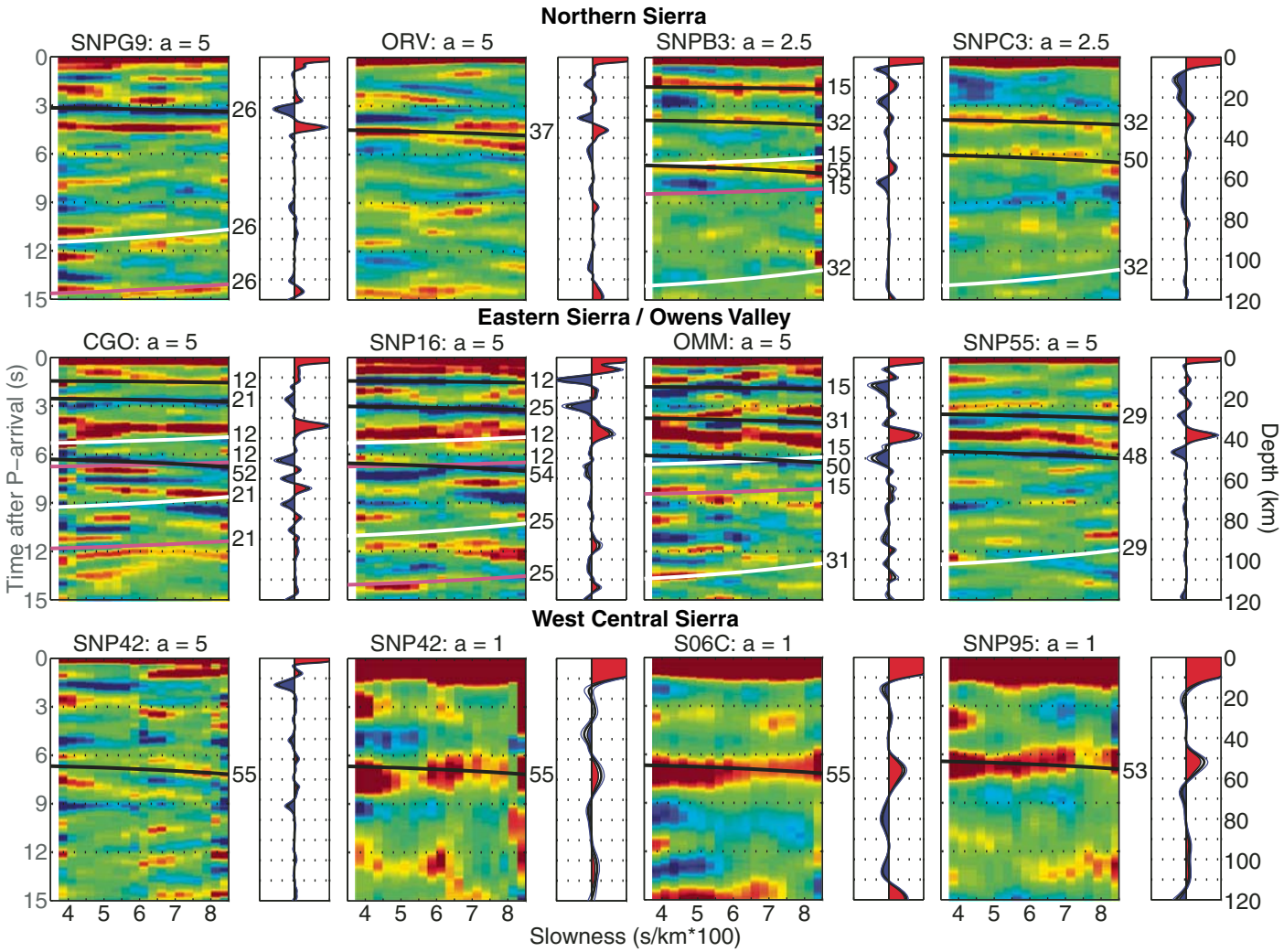

Figure 4. Receiver functions for selected stations unmigrated and stacked by slowness (distance) and migrated and summed. Move-out curves and depth conversion are calculated for Vp = 6.1 km/s, Vs = 3.53 km/s. For the move-out stacks, positive Ps conversions are red, negative Ps conversions are blue, and each color saturates at ±10% of the P arrival. Arrivals corresponding to Ps, 2P, and 2S are colored black, white, and magenta, respectively. Summed stacks are windowed around ±20% of the P arrival, with mean amplitudes (black) and bootstrapped error bounds (blue). Stations are grouped to demonstrate regional trends. Different *"a"* values are used to accentuate specific arrivals, including the Moho or other prominent conversions.

exhibited overwhelming reverberations from basins (e.g., MLAC, Ligorría and Ammon, 1999). The remaining data contain features in the structure of the crust and upper mantle that demonstrate both local coherence and regional variation. Receiver functions produced across SNEP show substantial variation in crustal thickness, amplitude of the Moho conversion, and presence of negative conversions in the crust and upper mantle. We evaluate the move-out pattern of shallowly sourced conversions, corresponding reverberations, and the Moho to discriminate between real and spurious structures and refine subsequent interpretations. Additionally receiver functions corrected for move out, migrated with a simple model, and summed per station provide a useful representation of local structure in depth (Fig. 4).

As a rule we identify the Moho as the largest regionally coherent conversion within the expected depth range of the continental crust-mantle boundary. Previous work (Zandt et al., 2004) defined a "Moho hole," or absence of strong conversions in this depth range, between the western batholith and Great Valley. Our observations extend this region to the northwest where stations show a lack of arrivals from 0 to 5 seconds followed by a diffuse conversion at 6–8 seconds. The conversion is resolvable at a = 1 but diminishes in amplitude at higher frequencies (Fig. 4)—a phenomenon we analyze later. Its move out is equivocal due to its long period, and is likely compounded by azimuthal variation in its depth being mapped into the move-out stacks (Fig. 5). These stations lack shallow structure, which could produce reverberations in this time range. We interpret these conversions as being generated by the Moho, deeper than 50 km and extending northward to ~38° N. In the northern foothills, several stations exhibit two positive arrivals in the expected range for the Moho. Eventually a single, shallower conversion becomes prominent across the northern Sierra Nevada.

Arrivals from the Moho are substantially more coherent, and appear robust for narrower Gaussians, across the eastern Sierra Nevada and Owens Valley. At high frequencies (a = 5) we clearly resolve Ps conversions from intracrustal structures. Coherent negative arrivals appear both above and below the Moho. These arrivals occasionally approach the amplitude of the Moho. Whereas reverberations generated in the upper crust may contribute to a few of the observed arrival patterns and are generally obvious in the corresponding CCP stacks, many stations are clear of interference from spurious arrivals and illustrate the presence of low wave-speed layers in both the crust and upper mantle. Arrivals from these structures increase in coherence at lower frequencies, and are imaged throughout the eastern half of the SNEP CCP stacks. Intracrustal conversions and a sharp Moho at high frequencies also occur in the northern Sierra Nevada and Basin and Range approaching the active Cascade arc.

Crustal Vp/Vs

The Vp/Vs (or Poisson's) ratio of a material relates directly to composition (Christensen, 1996), varies with geologic environment (Zandt and Ammon, 1995), and exerts significant control on estimating structure (Ammon et al., 1990). We use local earthquake arrivals, petrophysical models, and receiver functions to calculate crustal Vp/Vs across the Sierra Nevada. Unusually deep seismicity occurs beneath the west-central Sierra Nevada (e.g., Wong and Savage, 1983; Miller and Mooney, 1994; Pitt et al., 2002). These earthquakes frequently exceed 20 km in depth, vary in mechanism, and locate in a diffuse cluster north of Fresno near the boundary of the western batholith and the Foothills Metamorphic Belt and a confined zone near the southwestern edge of Yosemite National Park. We recorded and located many of these events (Hurd et al., 2006) and generated a Wadati diagram (e.g., Wadati, 1933; Hayes and Furlong, 2007) for a subset of 13 earthquakes occurring at 33.1–46.2 km depth to independently constrain Vp/Vs along these ray paths. Regression of arrivals from 214 event-station pairs yields a solution of ~1.72 and robust coefficient of determination (R^2) (Fig. 6). This demonstrates that the upper crust (<30 km) in the west-central Sierra Nevada is probably a homogeneous granitoid and within the range of Vp/Vs (1.71–1.76) for nearby tonalite samples (Fliedner et al., 2000).

To determine the elastic properties of the lower crust under the west-central Sierra Nevada batholith, we combine mineral modal proportions of Miocene-age xenoliths (Ducea and Saleeby, 1996) with the predicted mineral composition of arclogite from theoretical models (e.g., Saleeby et al., 2003). Integrating the known elastic responses of mineral grains comprising a rock with estimated pressure and temperature yields a corresponding petrophysical model. We use the major-element composition of clinopyroxene, orthopyroxene, garnet, and plagioclase from 13 xenoliths (Mihai Ducea, 2009, personal commun.) to calculate the proportions of mineral modes using the methodology presented in Klein and Hurlbut (1999) (Table 2). For determining the modes of garnet, we use a more specific calculator developed by Locock (2008). The averaged modal proportions of each mineral are translated into the modal proportions of residues predicted by thermodynamic models for melting basalt with 1% water at 1.0 and 1.5 GPa (Ducea, 2002; Saleeby et al., 2003). We multiply the observed proportions by the percentage of the total mineral in the residue and use an analytic macro (Hacker

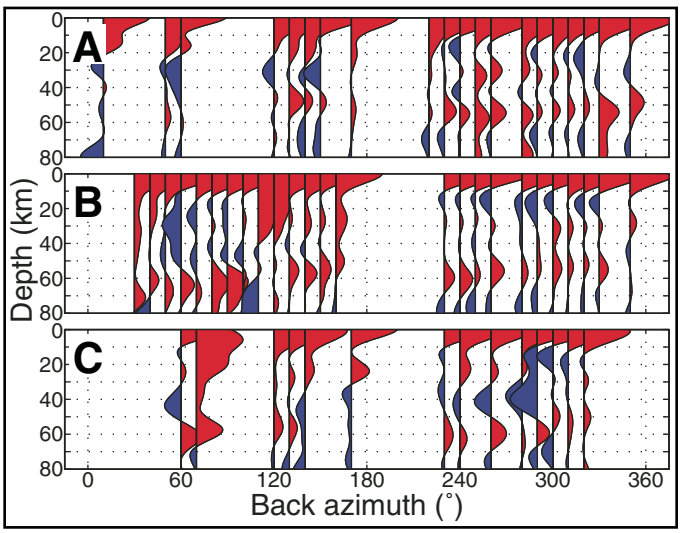

Figure 5. Migrated back-azimuthal stacks of stations (A—SNP95, B—S06C, C—SNP42) sampling deep Moho beneath the western batholith and Foothills Metamorphic Belt. Migrated for Vp = 6.1 km/s, Vs = 3.53 km/s. The Moho shows significant azimuthal variation for these stations, contributing to the ambiguous move out of the conversion (Fig. 4).

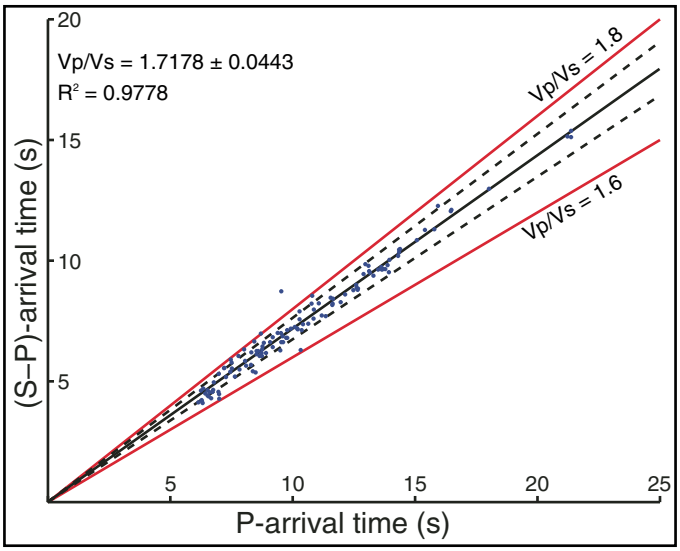

Figure 6. Wadati diagram and linear regression result for arrivals (blue) from 13 local events (Hurd et al., 2006). The range of error is the standard deviation of solutions calculated for individual event subsets.

and Abers, 2004) to calculate the density, Vp, and Vs for each rock.

From the preexisting thermodynamic constraints, we consider three garnet-clinopyroxenites and three mafic granulites generated by extracting melt fractions (F) of 0.15, 0.30, and 0.45 from hydrous basalt (Saleeby et al., 2003) (Table 3). The resulting residual rocks are dominated by >50% clinopyroxene, with varying amounts of garnet, orthopyroxene, plagioclase, and accessory hornblende (Ducea, 2002; Saleeby et al., 2003). As increasing proportions of melt are extracted from the system, the density of the residuum increases. The Vp/Vs ratio decreases slightly for mafic granulite, increases slightly for garnet-clinopyroxene, and ranges from 1.79–1.80 in all models. Both the garnet-clinopyroxenites (3509–3539 kg/m^3) and mafic granulites (3421–3432 kg/m^3) are dense relative to common peridotite (~3300 kg/m^3) (c.f. Ducea and Saleeby, 1996). The elastic parameters are relatively insensitive to background conditions; varying P and T by ±20% produces <1% change in Vp, Vs, Vp/Vs, and density. Additionally, the spread of calculated Vp/Vs is <0.01 despite a wide range of chosen values for P, T, and F for the six models.

TABLE 2. AVERAGED MAJOR ELEMENT COMPOSITIONS IN WEIGHT PERCENTAGE FOR MIOCENE-AGE XENOLITHS FROM THE CENTRAL SIERRA NEVADA*

Garnet	Granulite	Garnet-clinopyroxenite	Clinopyroxene	Granulite	Garnet-clinopyroxenite
SiO_2	39.7	40.5	SiO_2	50.9	53.7
Al_2O_3	22.2	22.1	Al_2O_3	3.2	4.3
TiO_2	0.1	0.1	TiO_2	0.5	0.3
Cr_2O_3	0.1	0.0	Cr_2O_3	0.1	0.1
FeO	18.0	19.4	FeO	10.9	5.1
MnO	1.1	0.4	MnO	0.4	0.0
MgO	10.4	11.4	MgO	11.7	13.8
CaO	8.7	6.5	CaO	21.1	21.2
Na_2O	0.2	0.0	Na_2O	1.1	1.5
Pyrope	38.5	39.9	Diopside	51.5	57.1
Almandine	33.7	40.0	Hedenburgite	36.6	28.0
Grossular	21.9	16.6	Jadeite	10.6	14.3
Orthopyroxene	Granulite	Garnet-clinopyroxenite	Plagioclase	Granulite	
SiO_2	51.6	55.4	SiO_2	56.8	
Al_2O_3	2.3	1.5	Al_2O_3	26.4	
TiO_2	0.1	0.0	CaO	9.0	
Cr_2O_3	0.0	0.0	Na_2O	5.9	
FeO	20.4	12.5	K_2O	1.2	
MnO	0.4	0.2			
MgO	24.3	30.7			
CaO	0.5	0.3			
Na_2O	0.0	0.0			
Enstatite	67.2	81.0	Albite	35.8	
Ferrosilite	31.7	18.4	Anorthite	47.0	
			Orthoclase	17.3	

*Mihai Ducea (2009, personal commun.).

Average crustal Vp/Vs may be calculated from the Moho conversion and its reverberations in receiver functions (Zandt et al., 1995). The EarthScope Automated Receiver Survey (EARS) (cf. Crotwell and Owens, 2005; http://ears.iris.washington.edu/stationList.html?netCode=XE05) uses automated H-K (crustal thickness-Vp/Vs) stacking (Zhu and Kanamori, 2000) for SNEP. Several stations located within the west-central batholith record Vp/Vs near 2.0, which is irregular given previous observations for felsic crust to ~30 km depth (Fliedner et al., 2000) and our Wadati diagram estimate. High Vp/Vs directs interpretations toward geologically implausible scenarios (e.g., melt-saturated, basaltic, or serpentinized crust). Weak signal from either the Moho or its reverberations limits the effectiveness of EARS, which weights the arrivals equally. Significant topography along the Moho also complicates H-K stacking (Hayes and Furlong, 2007; Lombardi et al., 2008), and the characteristics of the Moho beneath the central Sierra Nevada (Figs. 4 and 5) probably invalidate these Vp/Vs measurements. Other stations in the eastern Sierra Nevada and Owens Valley record Vp/Vs >2.0, which may result from constructive stacking of shallow mantle structure instead of reverberations.

The spacing of SNEP stations improves the 3-D resolution of the Moho and its 2P reverberation. User-defined picks for t_{Ps} and t_{PpPs} can be used to calculate Vp/Vs per CCP bin (e.g., Gilbert and Sheehan, 2004; Calkins et al., 2010). We migrate the CCP volume for t_{Ps} (a = 2.5) and the t_{PpPs} (a = 1) arrivals; the lowered *"a"* improves resolution of the reverberation. We stack with a variable Vp and constant Vp/Vs of 1.7; pseudodepths for the Moho are picked and then converted back to arrival times assuming a vertically incident ray for each bin (p = 0). Uncertainties from the picked depths are mapped into the error estimates for Vp/Vs at 294 out of 810 bins (36.3%), averaging to

TABLE 3. PETROPHYSICAL MODELS OF MAFIC-GRANULITES (A, B, C,) AND GARNET-CLINOPYROXENITES (D, E, F)

Volume (%)	A (0.15)	B (0.30)	C (0.45)	D (0.15)	E (0.30)	F (0.45)
Albite	5.0	4.6	3.2	1.1		
Anorthite	6.6	6.1	4.2	1.4		
Orthoclase	2.4	2.2	1.6	0.5		
Almandine	11.1	10.1	8.4	14.8	15.6	15.2
Grossular	7.2	6.6	5.5	6.1	6.5	6.3
Pyrope	12.7	11.5	9.6	14.8	15.6	15.2
Enstatite	0.7	4.7	6.7	4.9	3.2	0.0
Ferrosilite	0.3	2.2	3.2	1.1	0.7	0.0
Diopside	25.7	25.7	28.8	30.9	32.6	35.4
Hedenbergite	18.3	18.3	20.5	15.1	16.0	17.4
Jadeite	5.3	5.3	5.9	7.7	8.1	8.8
Hornblende	2.0					
Total	97.4	97.5	97.7	98.4	98.3	98.3
Pressure (GPa)	1	1	1	1.5	1.5	1.5
Temperature (°C)	600	600	600	800	800	800
Physical properties calculated with Hashin-Shtrikman average						
Vp (km/s)	7.70	7.68	7.67	7.88	7.96	7.96
Vs (km/s)	4.29	4.28	4.29	4.39	4.44	4.43
Vp/Vs	1.80	1.79	1.79	1.79	1.79	1.80
ρ (kg/m^3)	3421	3422	3432	3509	3539	3535

Note: Pressures consistent with Saleeby et al. (2003) and temperatures estimated from thermobarometry of xenoliths (Ducea and Saleeby, 1996).

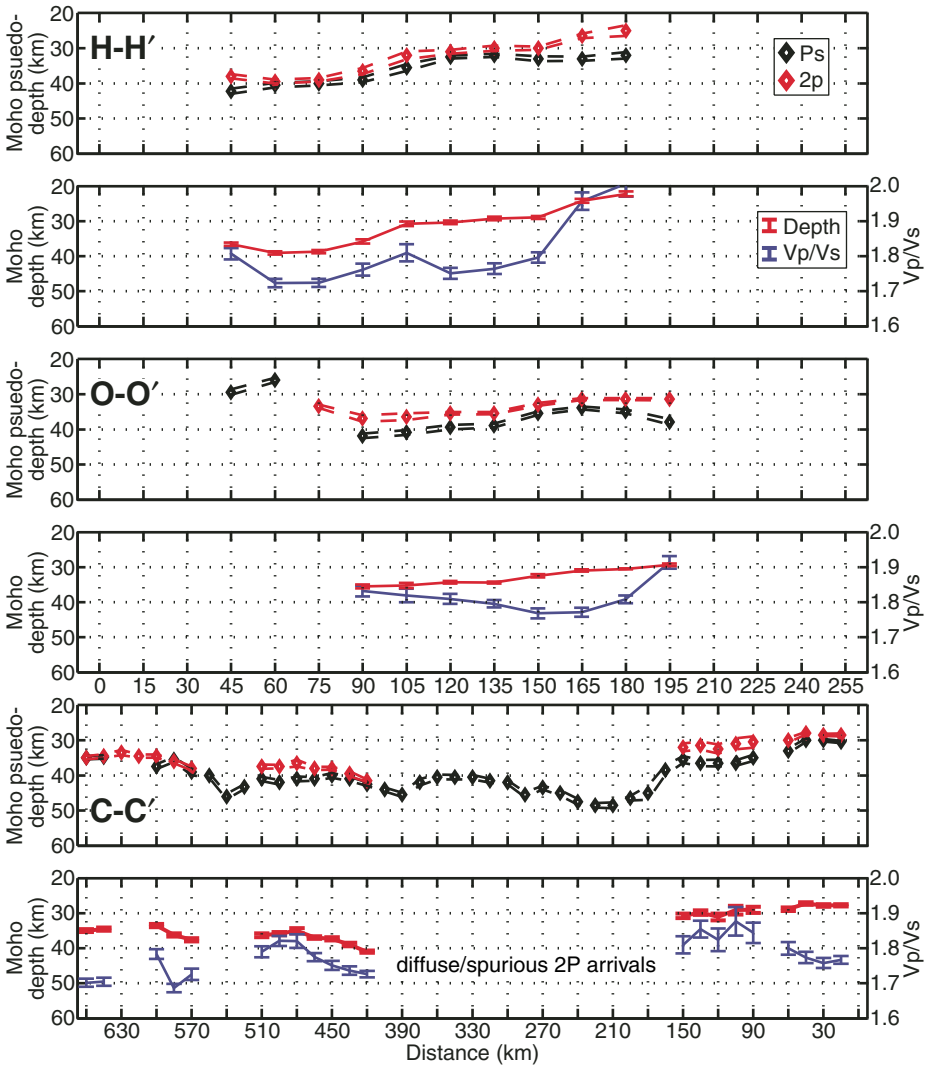

1.78 ± 0.01. Nearly all transects are discontinuous where picks are deemed unreliable and excluded (Fig. 7). Complex Moho structure in the northern foothills and central Sierra Nevada also precludes complete measurements, but the remainder of the Sierra Nevada and western Basin and Range are well covered.

The Wadati diagram and petrophysical models provide constraints where the unusual character of the Moho precludes measurements from receiver functions. We use all three data sets to create an integrated model of Vp/Vs, and in turn crustal composition, across the SNEP footprint. The combined measurements (Fig. 8) are largely consistent with surface geology. The Vp/Vs values measured across much of the batholith and adjacent Basin and Range are similar: 1.7–1.75 for receiver functions compared to ~1.72 from the Wadati diagram. These suit the measured average (1.73) for Mesozoic- and Cenozoic-age orogens (Zandt and Ammon, 1995), the value (~1.7) expected for the prevailing quartz- and feldspar-rich plutons (Christensen, 1996), and the local tonalite outcrops. Comparing measurements from the local earthquakes with petrophysical models shows a distinct increase of Vp/Vs with depth, reflecting the increasingly mafic composition of plutons emplaced beneath the Sierra Nevada (Saleeby et al., 2003). However, several pockets of unusually high Vp/Vs occur within SNEP, including the portions of the northern Sierra Nevada, southeastern Sierra Nevada, and the adjacent volcanic centers along Owens Valley (Fig. 7). In order to improve the accuracy of the CCP migration beneath the central Sierra Nevada, we fix Vp/Vs to 1.76 from averaging the deeper and shallower constraints. Observations drawn from "current" lithospheric material sampled by the xenoliths also provide important constraints when developing seismic forward models, as demonstrated later.

Characteristics of the Moho

The depth to the Moho varies considerably across this region (Fig. 9). Some of the thickest crust in North America is detected here, where the Moho is deeper than 40 km beneath the western batholith and Foothills Metamorphic Belt and exceeds 50 km depth within smaller zones. This feature is best resolved and most laterally coherent in receiver functions calculated

Figure 7. Moho depth (red) and Vp/Vs (blue) calculated from pseudodepth picks for the Ps and 2P arrivals on common–conversion-point transects.

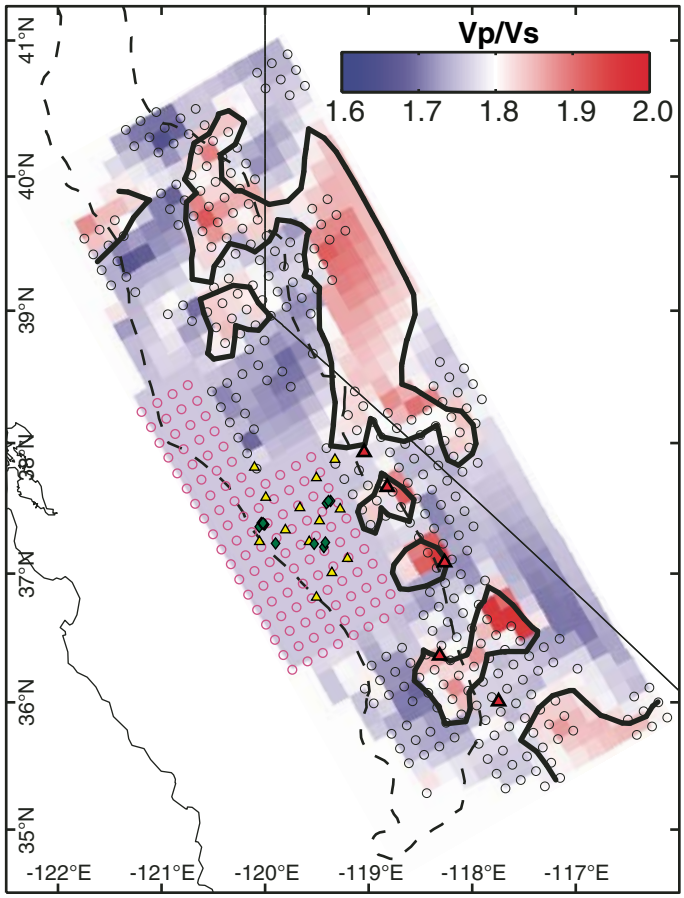

Figure 8. Vp/Vs measurements within the Sierra Nevada EarthScope Project footprint. Black circles show bins providing Vp/Vs from common–conversion-point analysis. Magenta circles represent Vp/Vs (1.76) derived using the combined results of the Wadati diagram and petrophysical models. We display stations (yellow triangles) that register arrivals from at least five events (green diamonds) for the Wadati diagram. Remaining points are interpolated using cubic approximation. Notable Quaternary-age volcanic centers are marked with red triangles. Lines mark the contoured Vp/Vs of 1.8.

for a = 1. Although previous studies (Jones and Phinney, 1998; Fliedner et al., 2000; Zandt et al., 2004) constrain 40+ km thick crust and imply the presence of a deep root (Louie et al., 2004), these results are the first to map a coherent deep conversion in this region.

The Moho shallows considerably away from the crustal welt. Conversions occur shallower than 35 km along the high Sierra Nevada. The crust generally thins across the eastern California shear zone and the northern Walker Lane to 25–30 km. This observation supports a compilation of crustal thickness estimates from controlled-source experiments (Heimgartner et al., 2006). The Moho ascends to ~20 km under the Foothills Metamorphic Belt adjacent to deeper Moho beneath the southern Foothills Metamorphic Belt and western batholith. The pronounced departure from a traditional style of Airy isostatic compensation beneath the region is a previously recognized paradox (e.g., Wernicke et al., 1996).

The amplitude of the Ps conversion from the Moho shows systematic geographic variation across the Sierra Nevada (Fig. 10). Low-amplitude arrivals denote a gradational or minor increase in wave speed and density across the Moho, whereas large amplitudes denote the opposite. For all three a values, the Moho is most sharply defined in the southern and eastern Sierra Nevada and Basin and Range, exceeding 40% of the P arrival amplitude in some areas. Conversely, its amplitude plummets under the deepest sections of the western batholith and Foothills Metamorphic Belt and is <10% of the P arrival throughout this region. Measurements of weak conversions and thick crust correlate closely.

Structural Transects

Along- and across-strike transects from the CCP stacks cover the entire Sierra Nevada (Fig. 2). On most transects the Moho appears clearly as a positive arrival. We select transects that portray the representative changes in the structure of the lithosphere across the Sierra Nevada and discuss receiver functions for a = 1 and a = 2.5. Our descriptions focus generally on the Moho and upper mantle structures in along-strike profiles and crustal features in across-strike profiles. We observe several dipping and vertically offset structures in these CCP stacks, representing regional changes in the structure of the Moho. Previous analysis of receiver functions in the southern Sierra Nevada includes resolution tests for the stacking parameters (Zandt et al., 2004, Supporting Information). These tests show that offset and dipping Moho structure may be discriminated for bins spaced 15 km apart. We use the same bin placement but a smaller bin radius than previously (20 km versus 30 km) to avoid excessively smearing arrivals and further reduce spurious signal with phase-weighting (Frassetto et al., 2010). The uniform coverage of SNEP stations across the Sierra Nevada, its lengthy deployment, use of more refined migration and stacking parameters should lead to robust resolution of structures beneath the array.

Sierra Nevada, Along Strike

The crust and upper mantle beneath the western Sierra Nevada adjacent to the Great Valley appear seismically homogeneous, with few prominent arrivals (Fig. 11 [A–A′]). A prominent Moho extends north from the Garlock fault, deepening and decreasing in amplitude under the central batholith and Foothills Metamorphic Belt. Reverberations from it appear at 130–150 km and stay distinct on eastward transects. There are also coherent arrivals in the upper mantle including a large negative to positive set of arrivals in the southern Sierra Nevada that may be a shallowly sourced reverberation. Beneath the northern foothills a clearly defined Moho dips northward to ~40 km depth. A diffuse negative conversion at ~70 km depth associates with the surface expression of the Foothills Metamorphic Belt here, but does not persist eastward. The two regions of visible Moho are separated by ~250 km of weak or absent conversions.

Low-frequency receiver functions resolve a mostly coherent arrival at 45–55 km depth farther east (Fig. 11 [B–B′]). The deepest and most

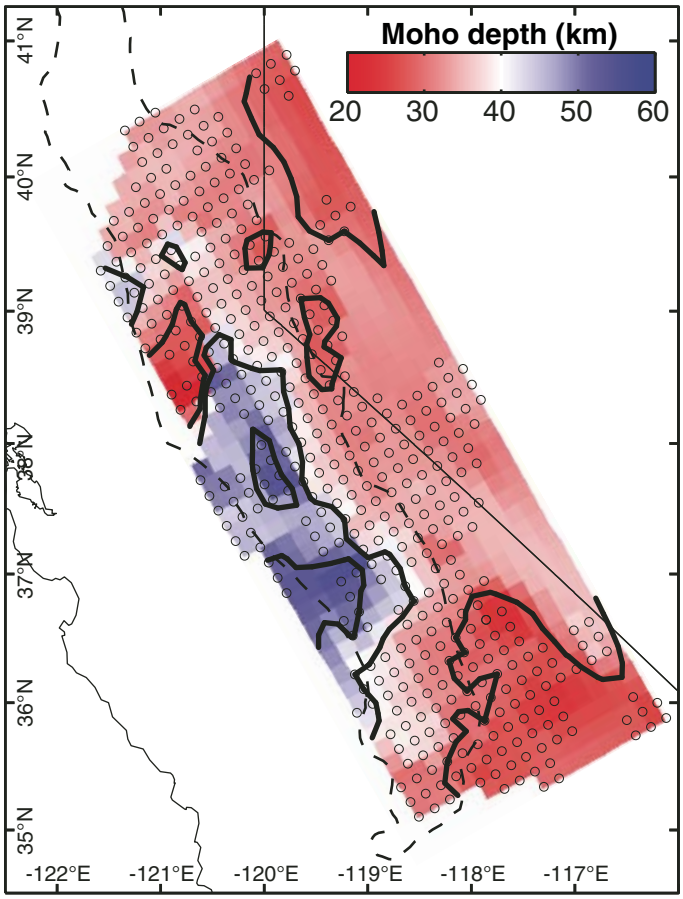

Figure 9. Moho depth below sea level for a = 1 mapped from common–conversion-point stacks. Lines mark the contoured depths at 30, 40, and 50 km.

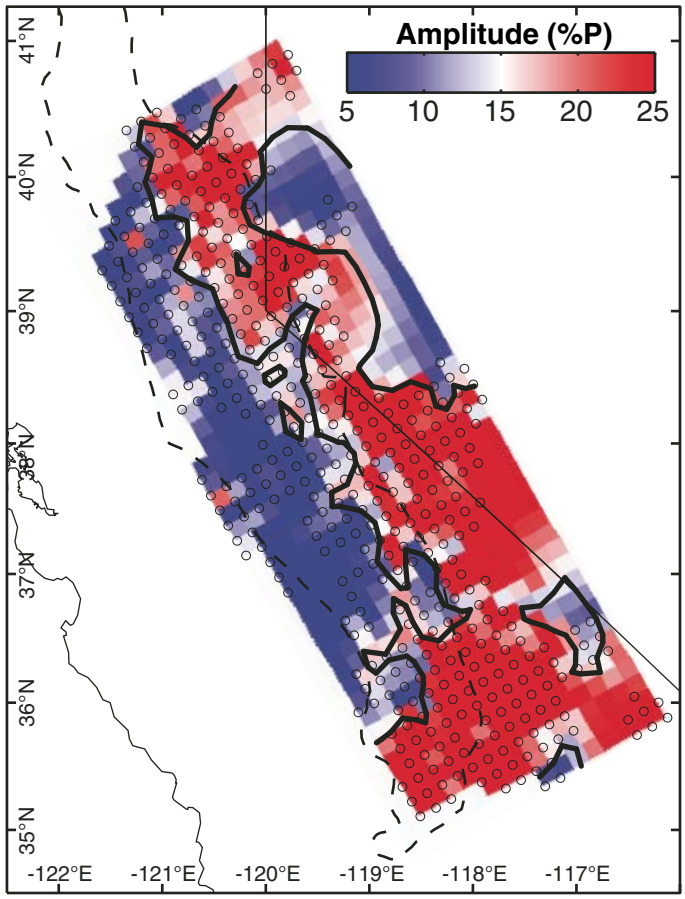

Figure 10. Amplitude of the Ps conversion from the Moho for a = 1 mapped from common–conversion-point stacks. Lines mark the contoured amplitude of 15% of the P arrival.

diffuse arrivals correlate well with the current location of the drip inferred beneath the western batholith and Great Valley (Figs. 1 and 11 [B–B′and C–C′]). The feature is not a reverberation from shallow structure (Fig. 4), and CCP bins containing this interface have coherent phase-weighting values in this range. Its proximity to the nearby shallow Moho beneath the northern foothills is contradictory, since there is no gravity anomaly that accounts for such a rapid shift in crustal thickness (Oliver, 1977). However, juxtaposing dense lower crust adjacent to typical upper mantle would minimize the density contrast despite the large discrepancy in the depth of the Moho.

Receiver functions sampling the high Sierra Nevada and adjacent Basin and Range display coherent and high-amplitude arrivals from the Moho along the length of the profiles (Fig. 11 [C–C′, D–D′, and E–E′]). There is no crustal root corresponding to the high elevation. Instead the crust is thickest in the west-central Sierra Nevada and thins outward. The Moho shallows to 30–35 km depth laterally along the crest (Fig. 11 [D–D′]). The Moho in the northern Sierra Nevada appears generally shallower and more coherent than in the central Sierra Nevada. There are some irregularities where in the northern Sierra Nevada it appears indistinct and potentially offset by ~10 km across a bin (Fig. 11 [C–C′]). This area contains some of the most densely faulted surface structure in the entire Foothills Metamorphic Belt with large outcrops of serpentinized oceanic peridotite (Fig. 1) (e.g., Saleeby, 1990).

The coherency and amplitude of conversions from mantle structure grow as SNEP extends into the adjacent Great Basin. High-amplitude, negative receiver-function arrival "bright spots" are prevalent beneath Owens Valley and the northern Walker Lane. The coherency of the negative arrival beneath the Moho (Fig. 11 [D–D′ and E–E′]) suggests that it may be a regional-scale feature. Deeper than 80 km we observe the 2P reverberations from the Moho, which appear throughout the upper mantle. However, in several areas another positive, direct conversion is visible from 80–100 km depth (e.g., Fig. 11 [E–E′]). We also observe this feature in move-out plots from stations in the eastern Sierra Nevada (Fig. 4), and it may result from the bottom of the slow layer modeled in regional waveforms (Savage et al., 2003).

Sierra Nevada, Across Strike

Receiver-function transects crossing the southernmost Sierra Nevada display a high-amplitude Moho dipping gently to the west-southwest (Fig. 12 [F–F′ and G–G′]). The Moho correlates well with subhorizontal structure interpreted from a controlled source profile collected to the south across the Tehachapi Mountains (Malin et al., 1995). Comparison to stations in the northern Mojave (Yan and Clayton, 2007) shows a regionally strong and coherent conversion from the Moho. This feature in the southernmost Sierra Nevada appears consistent with the establishment of a new, shallow Moho following the subduction of the Shatsky Rise, collapse of the overlying batholith, and development of a schist-rich lower crust from subducted detritus (e.g., Malin et al., 1995; Chapman et al.,

2010). The crust and upper mantle in the southernmost Sierra Nevada also contain several pronounced negative conversions across the width of the batholith. Continuing northward, the Moho remains flat beneath Owens Valley before increasing in depth westward beneath the high Sierra Nevada and dimming rapidly (Fig. 12 [I–I′]). The change in Moho depth beneath the southern Sierra Nevada appears as a step, and this region coincides with the downwarped and most diffuse section of Moho in the along-strike transects (Fig. 11 [B–B′, C–C′, and D–D′]). The hinge-line of deepening occurs roughly 30 km inboard of the eastern escarpment.

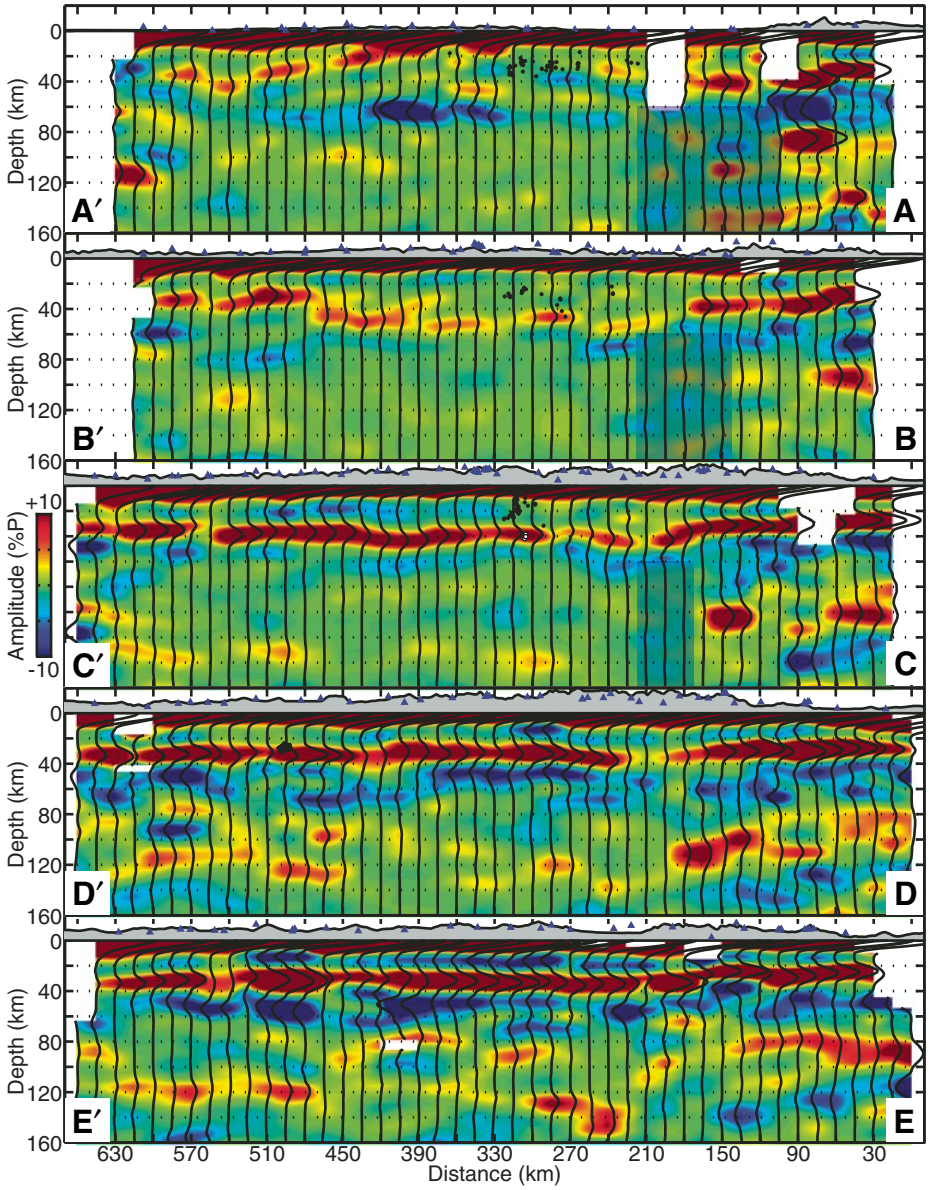

Figure 11. Sierra Nevada, along-strike, receiver-function transects for a = 1. Surface elevations are exaggerated five times. Stations marked on each transect are within one bin radius at the surface. A vertical projection of the Isabella anomaly at 125 km has transparent shading (Schmandt and Humphreys, 2010). The stacked receiver function for each bin is superimposed. Values between bins are interpolated linearly. Positive Ps conversions are red, negative Ps conversions are blue, and each color saturates at ±10% of the P arrival. Circles represent crustal earthquakes (black) and long-period earthquakes (white) occurring within one bin radius of each transect. Earthquakes in the west-central Sierra Nevada were located by Sierra Nevada EarthScope Project (Hurd et al., 2006) and near Lake Tahoe by a separate study (von Seggern et al., 2008).

The structural asymmetry becomes more pronounced moving northward beneath the high Sierra Nevada. The amount of conversions generated in the crust reduces noticeably from east to west. Almost no conversions in the middle to lower crust appear beneath the western batholith (Fig. 12 [H–H′, I–I′, J–J′, and K–K′]). In contrast bright spots concentrate beneath the eastern Sierra Nevada and particularly Owens Valley. A transect across the White Mountains (J–J′) shows a positive arrival overlying the lower crustal negative. This feature may relate to the zone of seismic anisotropy previously modeled in the lower crust (Zandt et al., 2004). Several of these arrivals may linger from shallowly sourced reverberations that survived stacking and phase-weighted filtering, particularly at the edges of the CCP volume. This is suggested by harmonic signals under Owens Valley (Fig. 12 [I–I′]) and western Nevada (Fig. 12 [L–L′]). However, move-out stacks (Fig. 4) demonstrate that stations situated nearby do show negative conversions generated by layering above and below the Moho.

A transect through Long Valley caldera and skirting southern Yosemite National Park (Fig. 2) shows that the changes in the character of the crust, Moho, and upper mantle may relate to unusually deep seismicity in the area (Fig. 12 [K–K′]). Earthquakes segregate into distinct clusters, one within the seismically homogenous crust above dimmed Moho near the Great Valley and the other a pipe-like feature atop where the prominent Moho terminates under the high Sierra Nevada (Hurd et al., 2006). Furthermore, that cluster locates above long-period earthquakes observed since 1994 that occur at the Moho (Pitt et al., 2002).

The overall structure of the crust and upper mantle becomes more complicated around 38° N. The unusual seismicity disappears but conversions from weak, deep Moho persist beneath the western foothills and axial batholith to near the latitude of Lake Tahoe (Fig. 12 [L–L′, M–M′, and N-N′]). The Moho dips to the west, deepening by ~20 km over five bin intervals, exceeding a 20° dip in some locations (Fig. 12 [N–N′]). This orientation likely relates to the unusual results from previous earthquake refraction analyses (Savage et al., 1994). To the west we observe an increase in the number and strength of conversions under the Foothills Metamorphic Belt. Beneath Lake Tahoe the lower crustal earthquake swarm of 2003 (Smith et al., 2004; von Seggern et al., 2008) overlies a bright, sharp Moho (Fig. 12 [O–O′]). However, some of this signal may relate to residual reverberations generated by the Lake Tahoe basin (cf. Frassetto et al., 2010).

The Moho dips more gently westward in the northern Sierra Nevada, nearing 40 km depth west-northwest of Lake Tahoe. Here it terminates sharply being offset by ~10 km from the Moho located beneath the northern foothills (Fig. 12 [O–O′ and P–P′]). This offset occurs beneath a heavily faulted region of the Foothills Metamorphic Belt, near the Melones fault zone (Fig. 1). As the SNEP array approaches the southern boundary of the Cascade Arc, a single, flat, consistently bright Moho becomes reestablished across the Sierra Nevada (Fig. 12 [Q–Q′]).

Depth Slices

We map the variation of CCP amplitudes to visualize the prominent changes in the character of the crust and upper mantle observed in the horizontal transects. Depths of ~15 and ~20 km feature bright spots above the Moho (Fig. 13). These are almost completely localized in the eastern Sierra Nevada with several occurring near volcanic centers. Amplitudes at greater depth (~50 km) show the large negative conversion most coherent at lower frequency (a = 1), distributing widely across the eastern Sierra Nevada and western Basin and Range (Fig. 13). Conversely the positive arrivals at the same levels in the west-central Sierra Nevada show the weak arrivals from the Moho, emphasizing the steep westward dip of the crust-mantle boundary and general asymmetry of crustal thickness and structure across the range.

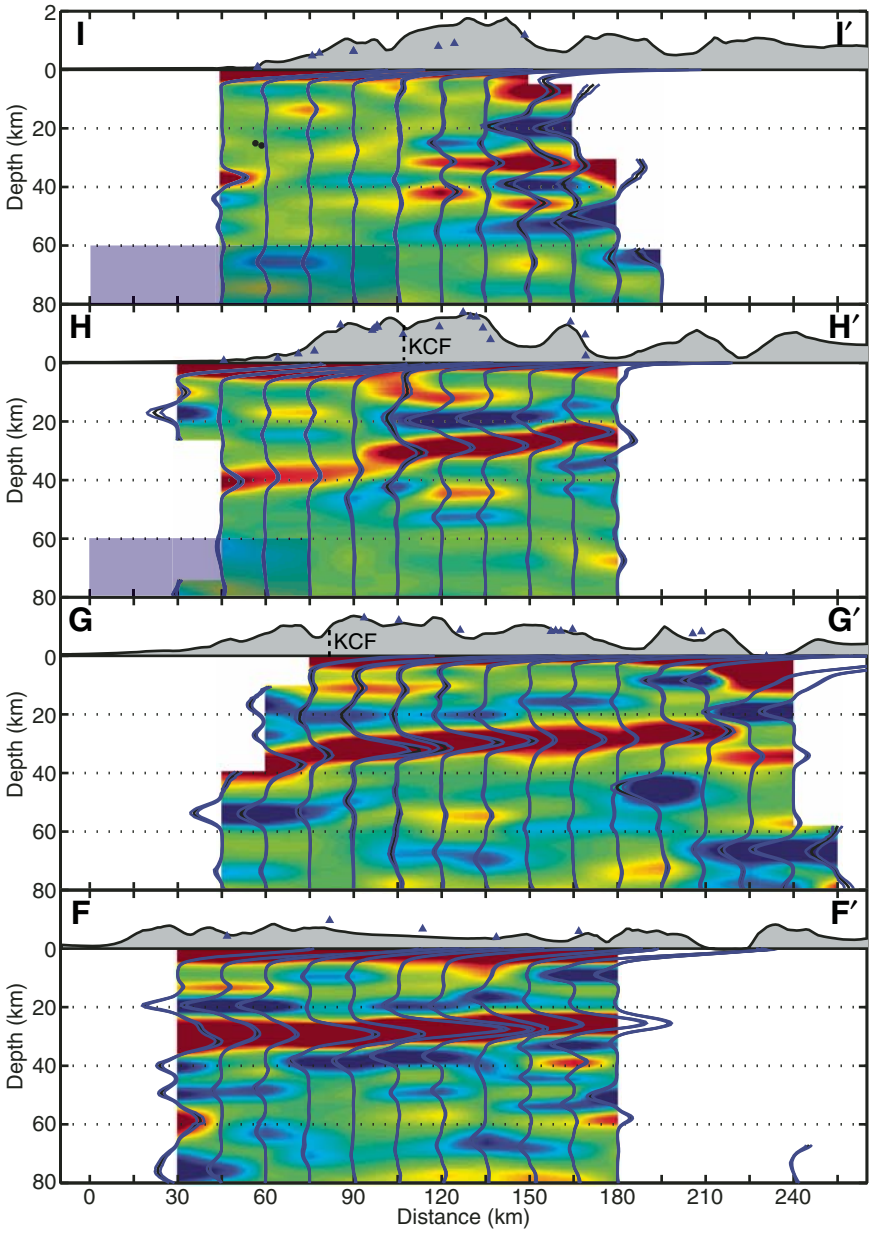

Figure 12 (*continued on following pages*). Sierra Nevada, across-strike, receiver-function transects for a = 2.5. A vertical projection of the Isabella anomaly from 125 km (Schmandt and Humphreys, 2010) has transparent shading. The mean receiver function (black) and its bootstrapped ±1σ error bars (blue) for each bin are superimposed. Arrows mark the approximate boundary between the Foothills Metamorphic Belt and axial Sierra Batholith. KCF—Kern Canyon fault, MFZ—Melones fault zone, HLF—Honey Lake fault.

DISCUSSION AND MODELING

Relation to Surface Geology and Structures

Trends in both Vp/Vs and seismic structure link to regional expressions in basement geology and faulting. In the southern Sierra Nevada, projecting the trace of the proto–Kern Canyon fault–Kern Canyon fault (Fig. 1) (Parrish, 2006; Nadin and Saleeby, 2008) truncates a negative conversion in the lower crust and intersects a step in the Moho of ~8 km between stacking bins (Fig. 12 [H–H′]). The offset is visible in the directional arrival pattern for a nearby station (Fig. 14B). Receiver functions from here modeled anisotropic lower crust, potentially associated with deformation during lithospheric foundering (Zandt et al., 2004, Supporting Information). In that case, the observed Moho offset is not produced by the modeled anisotropic layering.

This irregular Moho represents a boundary between intact and extended crust within the southern Sierra Nevada (Fig. 14). The batholith south of ~36° exhibits increasingly exhumed basement approaching the Garlock fault (cf. Nadin and Saleeby, 2008). Moreover, ubiquitous extensional structures appear only east from the Kern Canyon fault at this latitude and southward. The distribution, age, and location of these structures suggest that overlying crustal material was tectonically removed southward during extension associated with the channelized extrusion of subcreted schist (Chapman et al., 2010), and now correlates with the upper plate of batholith presently dispersed across the northern Mojave (Wood and Saleeby, 1998). Thermochronologic data (Mahéo et al., 2009; Wood and Saleeby, 1998) identifies rapid cooling of lower-plate basement in the late Cretaceous, near the breakaway zone, just south of transect H–H′.

The offset Moho introduced by this crustal thinning exclusively to the east of the Kern

Canyon fault appears to have lasted until present, and the nearby Isabella breakaway zone shows evidence for Neogene- to Quaternary-age extensional reactivation (Mahéo et al., 2009; Saleeby et al., 2009). This style of reactivation is observed in focal mechanisms from a swarm of earthquakes confined to the east of the Kern Canyon fault (Jones and Dollar, 1986) that exhibit purely normal faulting. The structural offset emphasizes the changing amplitude of the Moho, which transitions from a strong conversion occurring beneath the eastern Sierra Nevada to a relatively weaker conversion to the west of the Kern Canyon fault. Additionally, Vp/Vs values are generally higher east of the Kern Canyon fault (Fig. 8). Postdelamination magmatism and extension would enhance the Moho by lowering the wave speed of the lower crust and increasing Vp/Vs, but the lack of young faulting or seismicity west of the offset demonstrates that significant extension has yet to occur beyond the Kern Canyon fault (Saleeby et al., 2009). The lack of Miocene-age or younger volcanism in this "avolcanic corridor" supports this interpretation as well (Farmer et al., 2002).

The crust becomes increasingly complicated in the central and northern Foothills Metamorphic Belt, as folds and thrusts bound a collage of ophiolitic, serpentinized ultramafic rocks, metamorphosed terranes, and batholithic plutons (Schweickert et al., 1984; Saleeby, 1990; Saleeby, 1992; Parrish, 2006). Crustal Ps conversions increase with the surface exposure of the Foothills Metamorphic Belt (Figs. 1 and 12 [L–L′, M–M′, and N–N′]) and may relate to the crustal structure observed farther north and inferred to extend along the foothills (Spieth et al., 1981). Other previously observed structures (Miller and Mooney, 1994) lie outside our station coverage. A positive Ps at 20–25 km depth overlies deep Moho beneath the Foothills Metamorphic Belt (Fig. 12 [N–N′]) on several transects before eventually transitioning into a single Moho beneath the northern foothills (Fig. 12 [O–O′]). The along-strike transects clearly show this structure dipping northward (Fig. 11 [A–A′]) (Fig. 15). Stacks for different Gaussians record the transition between shallow and deep Moho beneath the western extent of SNEP (Fig. 15). For $a = 2.5$, these features overlap for >200 km, and the layer between them is at least 15 km thick.

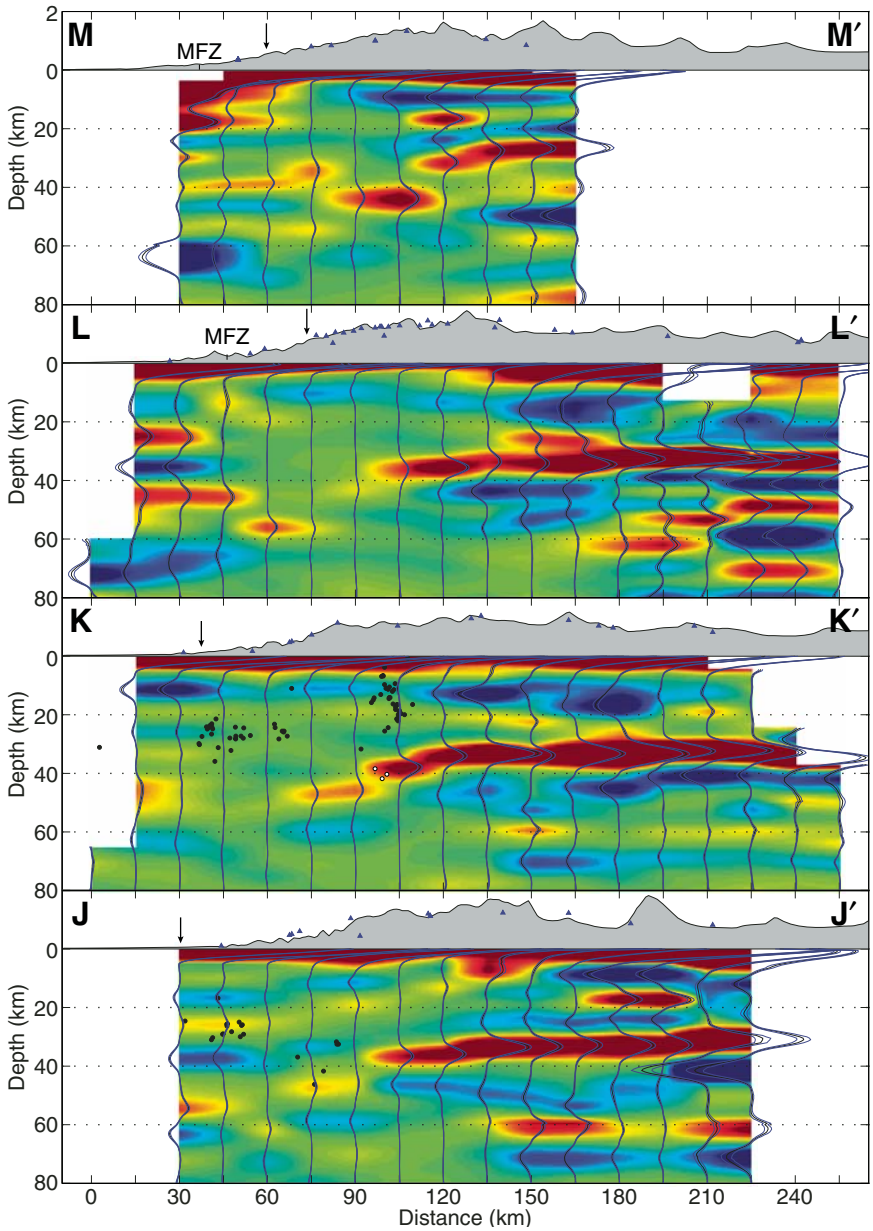

Figure 12 (*continued*).

The Moho beneath the Foothills Metamorphic Belt shows abrupt change in crustal thickness for $a = 1$ (Fig. 11 [B–B′]) (Fig. 15). However, Bouguer gravity and refraction modeling in the region show little evidence for such an extreme offset in the Moho (Oliver, 1977; Louie et al., 2004). The adjacent and overlapping styles of Moho may serve as a gradual transition between sections of the Sierra Nevada that evolved differently as an arc. The amount of exposed Cretaceous-age plutons decreases in the northern Sierra Nevada as the batholith turns eastward into Nevada (Barton and Hanson, 1989) (Fig. 1). We suggest that the shallower structure (Fig. 15) is preexisting Jurassic-age Moho. This feature is coherent and mappable in several transects to the north, but is less well defined across the central foothills. Numerous sheeted dike complexes located along the Foothills Metamorphic Belt and western batholith suggest that the entire region underwent considerable extension during the Jurassic (Wolf and Saleeby, 1992). We assert that this structure represents the postextension continental Moho prior to final emplacement of the batholith. We interpret the deeper layer (Fig. 15) as a Cretaceous-age Moho coincident with granitoid melts that disrupted and overprinted the earlier Moho as the density of plutons increased, eventually obscuring the previous crust-mantle boundary throughout the central Sierra Nevada. Since Cretaceous-age plutons are much less prevalent in the northern Foothills Metamorphic Belt, the preexisting Moho is better preserved.

Disruptions in the Moho correlate with the Melones fault zone and other surface faulting

within the Foothills Metamorphic Belt (Figs. 11 [C–C′] and 12 [O–O′ and P–P′]). The north-south–striking fault zone presents the boundary between Paleozoic-age accreted lithosphere and the older North American passive margin truncated by transform movement (e.g., Saleeby, 1990). This feature is only visible across a few CCP transects, but appears robust due to the absence of shallow structure and the corresponding potential for reverberations. Unfortunately the placement of stations here does not yield a location that directly samples the offset structure, unlike in the southern Sierra Nevada. The position of the largest Moho offset (Fig. 12 [P–P′]) crossing the Sierra Nevada matches noticeable changes in crustal structure near the 75 km distance marker for profiles to the north and south (Fig. 12 [O–O′ and Q–Q′]). The Moho along and across strike beneath the northern Foothills Metamorphic Belt appears to have inherited structures associated with the prebatholithic assemblage of continental material here.

Uncertainty remains regarding the development of a large corresponding arclogite in the northern Sierra Nevada. A lack of xenoliths prevents directly sampling the lower crust and mantle lithosphere. The location of the Sr 0.706 line (e.g., Armstrong et al., 1977) in the central Sierra Nevada places the melting zone of the northern batholith within oceanic lithosphere, potentially limiting the production of garnet-rich phases (e.g., Ducea and Saleeby, 1998a). The distribution of batholithic plutons in the northern Sierra Nevada (Saleeby et al., 1989) and in the northern Great Valley subsurface (May and Hewitt, 1948; Williams and Curtis, 1977; Harwood and Helley, 1987; Saleeby, 2007) indicates that arc plutonism in the early Cretaceous was dispersed over a wide belt with a relative abundance of hosting metamorphic wall rocks as compared to the south. Plutons in northwestern Nevada show that significant amounts of arc magmatism in the late Cretaceous occurred to the east of the northern geographic Sierra Nevada (Barton and Hanson, 1989; Van Buer et al., 2009). Estimates of Cenozoic-age extension reveal that the crust within the Mesozoic-age arc in Nevada has not been significantly stretched, and appears <40 km thick at ca. 90 Ma (Colgan et al., 2006a, 2006b). Alternatively the northern Sierra Nevada batholith may have developed an eclogitic residue that subsequently foundered and occupies the nearby "Redding anomaly" (Jones et al., 2004). However, under such a circumstance the type of particularly high-amplitude Moho conversion associated with the aftermath of lithospheric foundering to the south is limited in extent or entirely absent in the north.

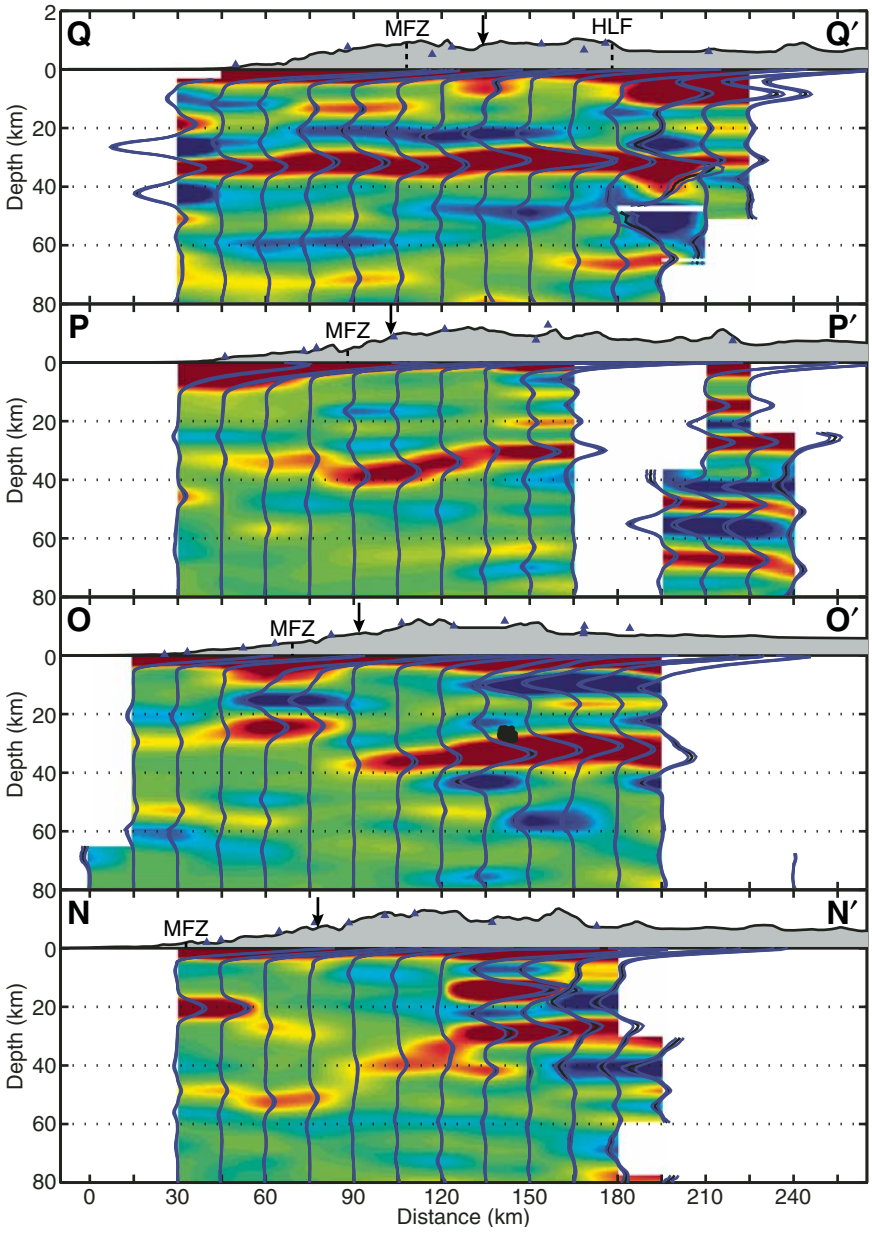

Figure 12 (*continued*).

We later discuss high Vp/Vs measurements in the eastern Sierra Nevada in the context of volcanic features, but similar findings within the northern Sierra Nevada do not correspond to major Quaternary-age volcanic centers (Fig. 8). Three distinct zones of Vp/Vs >1.8 may link to serpentinized ophiolites (Saleeby, 1990) that outcrop amidst Paleozoic metamorphic rocks to the northwest of Lake Tahoe (Fig. 1). Serpentinite contains extremely high Vp/Vs (>2.0 in laboratory measurements) but also a low Vp of ~5.5 km/s (Christensen, 1996). Regional tomography finds small reductions in crustal Vp but no large-scale anomalies near the location of these elevated Vp/Vs measurements (Thurber et al., 2009). Christensen (1996) shows that the Vp and Vp/Vs of an average serpentinite at 200 MPa deviate respectively by ~15% (5.308 km/s versus 6.246 km/s) and ~17% (2.051 versus 1.702) from typical plutonic rock (granite-granodiorite). Observed Vp/Vs increases in these regions may reflect the presence of serpentinized crustal material, but a large-scale presence seems unlikely since reduced Vp is not observed. This comparison is hampered by the complex geologic history of these rocks, which contain large amounts of oceanic peridotite and record increasing metamorphic grade subsequent to partial serpentinization (e.g., Saleeby, 1990). Alternatively, the easternmost of these high Vp/Vs zones may relate to the migration of arc-related volcanism

through the northern Sierra Nevada within the past ca. 5 Ma (Cousens et al., 2008). Along the border of the Sierra Nevada and northern Walker Lane, the Honey Lake fault (Parrish, 2006) truncates a shallow, positive conversion to the east (Fig. 12 [Q–Q′]), emphasizing a sharp boundary between the physiographic provinces that is otherwise not clearly defined along the eastern boundary of SNEP.

Magma Bodies and Related Earthquakes

The CCP stacks and crustal Vp/Vs measurements show considerable evidence for zones of partial melt in the crust and upper mantle along the eastern Sierra Nevada and Walker Lane. Temperatures in the lithosphere rapidly increase from eastward (Blackwell and Richards, 2004), and the boundary between high and low heat flow coincides geographically with the western edge of the bright spots (Fig. 13). The lateral coherency and sharp negative amplitude of the deeper boundary at ~50 km likely coincides with the lithosphere-asthenosphere boundary (LAB) in this region (Fig. 13). Other recent observations of lithospheric thickness from sparser data place the LAB at 60–70 km beneath the eastern Sierra Nevada (Li et al., 2007). However, thermobarometry of nearby xenoliths defines an adiabat and temperatures approaching 1250 °C at depths of 35–40 km, coincident with the Moho mapped with receiver functions, beneath Owens Valley (Ducea and Saleeby, 1996).

Bright spots at 15–20 km depth coincide with existing geophysical evidence of magma bodies and surface expressions of Quaternary-age volcanism, including the Death Valley Bright Spot (de Voogd et al., 1986), Long Valley, and Mono Craters, and the Coso, Big Pine, and Golden Trout volcanic fields near and within Owens Valley (e.g., Manley et al., 2000) (Fig. 13). Near Coso we also detect the shallow magma body imaged previously with receiver functions (Wilson et al., 2003). Previous observations of inferred midcrustal magma at Death Valley and Socorro, New Mexico, occur at similar depths of ~15–20 km (de Voogd et al., 1986), and receiver functions from Soccoro (Sheetz and Schlue, 1992) have similar amplitudes. Pockets of crustal Vp/Vs >1.85 appear near Long Valley, Big Pine, and Golden Trout volcanic fields (Fig. 8) and correlate closely with the negative arrivals in CCP transects, providing further evidence toward interpreting certain prominent negative conversions as the upper surfaces of partial melt. While conductivity observations in the southern Sierra Nevada call for high temperatures but not widespread partial melt within the crust and upper mantle, some do corroborate ~3% partial melt beneath Miocene-age and younger volcanic centers (Park, 2004).

Earthquakes occurring beneath northern Lake Tahoe (von Seggern et al., 2008) and southern Yosemite National Park (Pitt et al., 2002) may result from the intrusion of basaltic melt into the lower crust. On CCP transects the sequence of earthquakes near Lake Tahoe locates ~5 km above the Moho (Fig. 12 [O–O′]). However, those in southern Yosemite occur directly along the Moho where it switches abruptly from a well-defined arrival at ~40 km depth to a deeper, weaker conversion westward (Fig. 12 [K–K′]). Neither cluster of seismicity locates directly within a negative arrival, but they may relate to other features resolved in each transect. The seismicity in northern Lake Tahoe underlies a small negative Ps, which may be the eastward continuation of a significant slow layer resolved by regional tomography (Thurber et al., 2009). The Moho-depth earthquakes below Yosemite occur just beyond the western terminus of the regional bright zone in the upper mantle. Both clusters of seismicity are recently constrained features that merit further study; similar earthquakes within the Ethiopian Rift result from magma injection from mantle rich in partial melt.

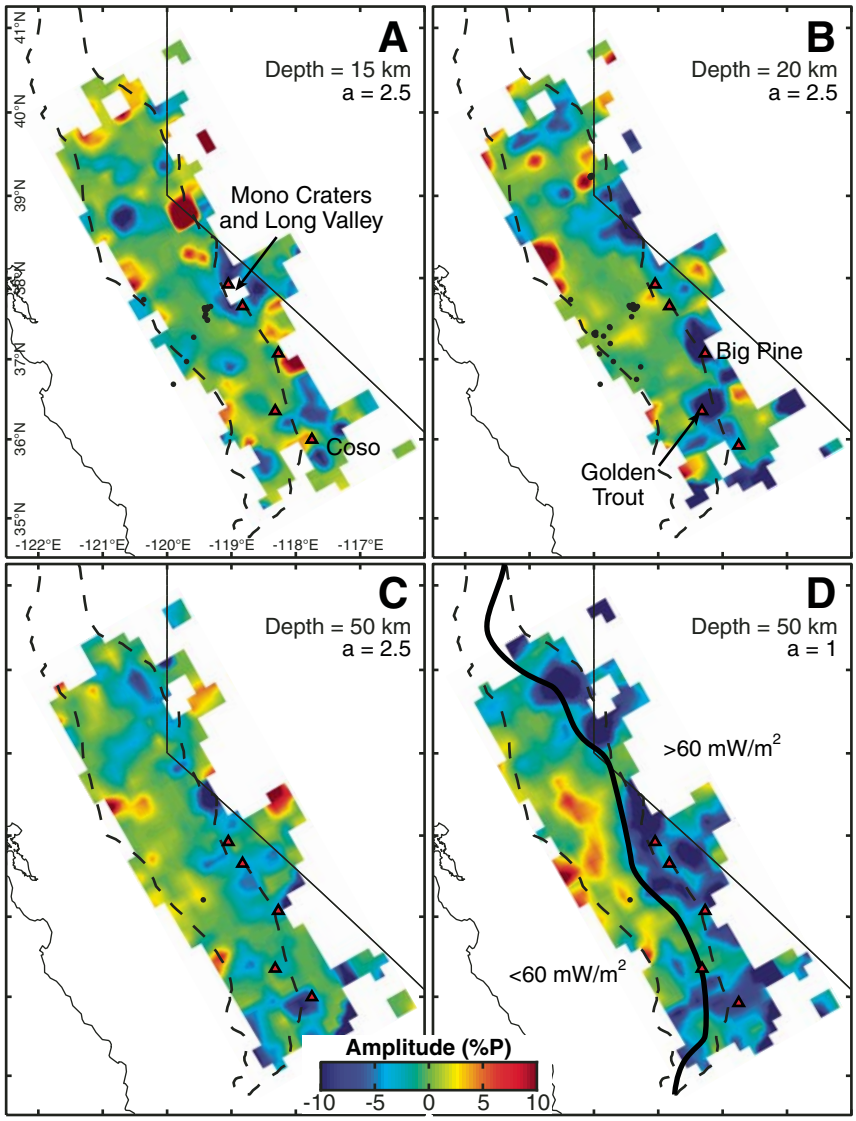

Figure 13. Receiver-function slices by depth for *a* = 2.5 (top) and *a* = 1 (bottom). Black circles represent seismicity occurring ± 2.5 km from each depth. Notable Quaternary-age volcanic centers are marked with triangles and labeled. The black line marks the 60 mW/m² isocontour for reduced heat flow (Blackwell and Richards, 2004).

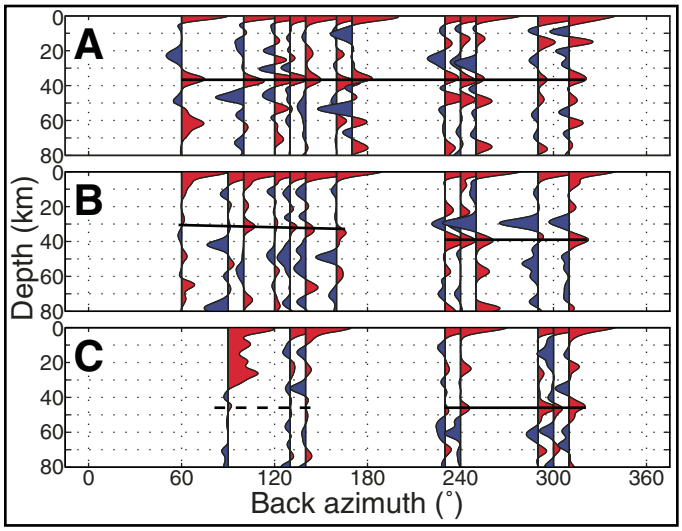

Figure 14. Migrated back-azimuthal stacks of stations (A—WHP, B—JUN, C—CCC) crossing the Kern Canyon fault from east to west. Migrated for Vp = 6.1 km/s, Vs = 3.53 km/s.

Moho Sharpness and Sensitivity

The drastic regional change in the depth and amplitude of the Moho stands as one of the most intriguing findings of SNEP. Low-frequency receiver functions effectively map the Moho as a deep interface where it went undetected previously (e.g., Fliedner et al., 1996; Zandt et al., 2004). Its conversions beneath the west-central Sierra Nevada become progressively weaker at high frequencies and almost indistinguishable at $a = 5$ (Fig. 15). Previous studies note the increased coherence of the continental Moho at lower frequencies (Owens and Zandt, 1985; Calkins et al., 2006), but in these cases its conversion remained discernable at higher frequencies (e.g., $a = 5$). The relative invisibility of this portion of Moho demonstrates the drawback of limiting a receiver-function data set to a single a value and motivates processing and evaluating both higher and lower frequency data.

We consider three models for the increase in Vp, Vs, and density across the boundary; a step and constant gradients of 10 and 20 km in thickness. Using the ray-tracing code *ray3d* (Owens et al., 1984) to generate synthetic seismograms for these models, we calculate the corresponding receiver functions for $a = 1$, 2.5, and 5. The subsequent stacks (Fig. 16) demonstrate the range of responses for combinations of frequency range and boundary thickness. For gradients in wave speed, different Gaussians resolve the same transition with different amplitudes. In the case of a sharp transition, it remains clearly defined across all frequencies. For the most gradual transition, even receiver functions using $a = 2.5$ resolve less than half of the peak amplitude obtained with $a = 1$. When $a = 5$, the conversion from the Moho is one-fourth the amplitude of $a = 1$. The low amplitude and irregularity of these features at high frequencies in our observations increases their chance of being missed.

We apply this assessment to SNEP by comparing different a-values from CCP bins sampling inside and outside the region of weak conversions from the Moho. We focus on an across-strike transect from the central Sierra Nevada, which traverses the rapid change between different styles of Moho (Fig. 12 [K–K′]). The response in selected stacks from east to west (Fig. 17) mirrors that of the synthetic data. The Moho beneath the eastern Sierra Nevada and Walker Lane remains clearly resolvable for $a = 5$, but only receiver functions for $a = 1$ retain significant amplitude beneath the western batholith. The relative difficulty of observing the Moho at high frequencies here suggests that the Moho under the west-central Sierra Nevada represents a gradual transition of significant thickness between the crust and upper mantle that may only be resolved by frequencies low enough to detect thick gradients in wave speed.

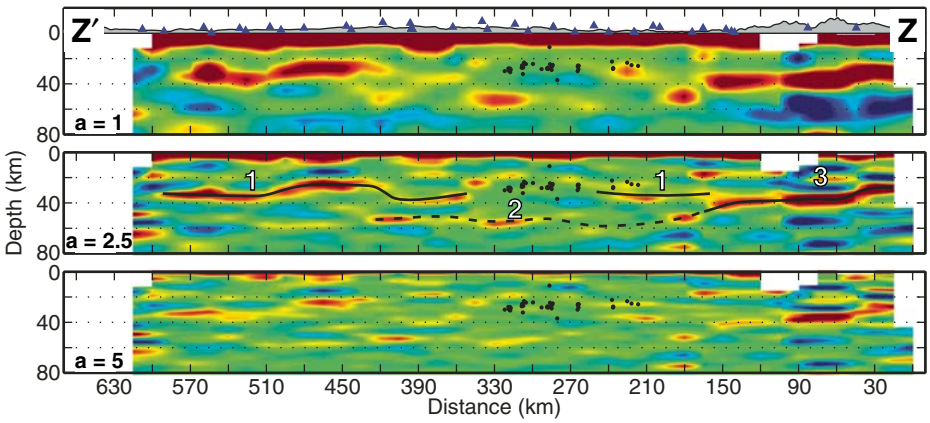

Figure 15. Along-strike, receiver-function transects through the foothills for $a = 1$ (top), $a = 2.5$ (middle), and $a = 5$ (bottom). Three different styles of Ps conversion from the Moho are traced and numbered: 1—Jurassic-age extensional Moho; 2—Cretaceous-age batholithic Moho; 3—Cenozoic-age Moho.

Seismic Forward Modeling

Deep, gradational Moho underlying seismically homogeneous crust juxtaposed against shallower, sharp Moho bounded by bright spots illustrates the drastic change in the structure of the lithosphere and thickness of the crust over relatively short distances beneath the central Sierra Nevada. Since this transition occurs within the batholith, we infer that it results from continued lithospheric foundering, which has largely concluded beneath the southern Sierra Nevada (e.g., Zandt et al., 2004). Body-wave and surface-wave tomography generated using SNEP (Gilbert et al., 2008; Reeg et al., 2008; Schmandt and Humphreys, 2010) resolves a region of high wave speed that almost exactly matches the geographic distribution of weak Moho and extends to depths of 70–90 km. In contrast, the same depths in the eastern Sierra Nevada and adjacent Basin and Range exhibit considerably lower wave speeds. Evidence presented throughout this study signifies intact arclogite beneath the west-central Sierra Nevada and shallow asthenosphere where this

material has foundered beneath the eastern Sierra Nevada.

Forward-modeling a CCP transect tests this interpretation, and allows us to match changes in structure of the crust and upper mantle to viable models. We use an across-strike transect that borders southern Yosemite National Park and Long Valley caldera (Fig. 12 [K–K′]), which bisects the region where we interpret foundering to be in progress. Our synthetic data set (a = 2.5) comprises a ten-station transect that samples five models to represent the crust and upper mantle (Fig. 18). We calculate synthetic seismograms for an incident P wave and its P-to-S conversions over a range of ray parameters (0.04, 0.05, 0.06, 0.07, and 0.08 s/km) and back azimuths (30° increments). The models are designed to fit the amplitudes of the CCP transect and are guided by Vp, Vs, and density derived from local xenoliths (Table 2), parameters from controlled-source surveying and laboratory analysis of plutons (Fliedner et al., 2000), and our observations of Vp/Vs and crustal thickness. The average Vp for the upper crust is close to a previously developed model for the region (Miller and Mooney, 1994). For the western batholith and Foothills Metamorphic Belt we assign a gentle gradient to represent a gradual transition with depth from tonalite through mafic granulite to garnet-clinopyroxenite, representing the products from the climactic arc flare-up in the Sierra Nevada (e.g., Saleeby et al., 2003). For the Walker Lane models, gradients are sharp between large-scale discontinuities in order to effectively fit amplitudes for the much sharper crust-mantle boundary and prevalent bright spots. We model the bright spots as layers with reduced Vs and elevated Vp/Vs to represent regions of partial melt. We process and stack the receiver functions using the same parameters as the SNEP data set.

The modeled transect generally matches the geographic distribution and amplitude of prominent conversions (Fig. 18). Although the details in these models are nonunique, the general features are well constrained. Models representing the western portion require a 6%–7% step in Vs over 4–8 km to reproduce the observed Moho conversion. This is embedded within a steady gradient of increasing wave speeds and density. The lack of conversions in the center of the observed zone of weak Moho requires a constant gradient throughout the crust. For the Moho to the east, increases of 19%–24% over 1 km reproduce the sharp Moho. We require large reductions (18% and 6%) in the midcrust and upper mantle to mimic the bright spots seen near Long Valley caldera. The substantial decrease in wave speed needed to match the negative conversions is unlikely to be due to merely compositional or temperature changes and is most likely produced by the presence of melt. The proximity of the Long Valley caldera and its inferred magma chamber make this explanation reasonable. Electrically conductive crust mapped just north of this region supports the presence of crustal magma (Ostos and Park, 2008).

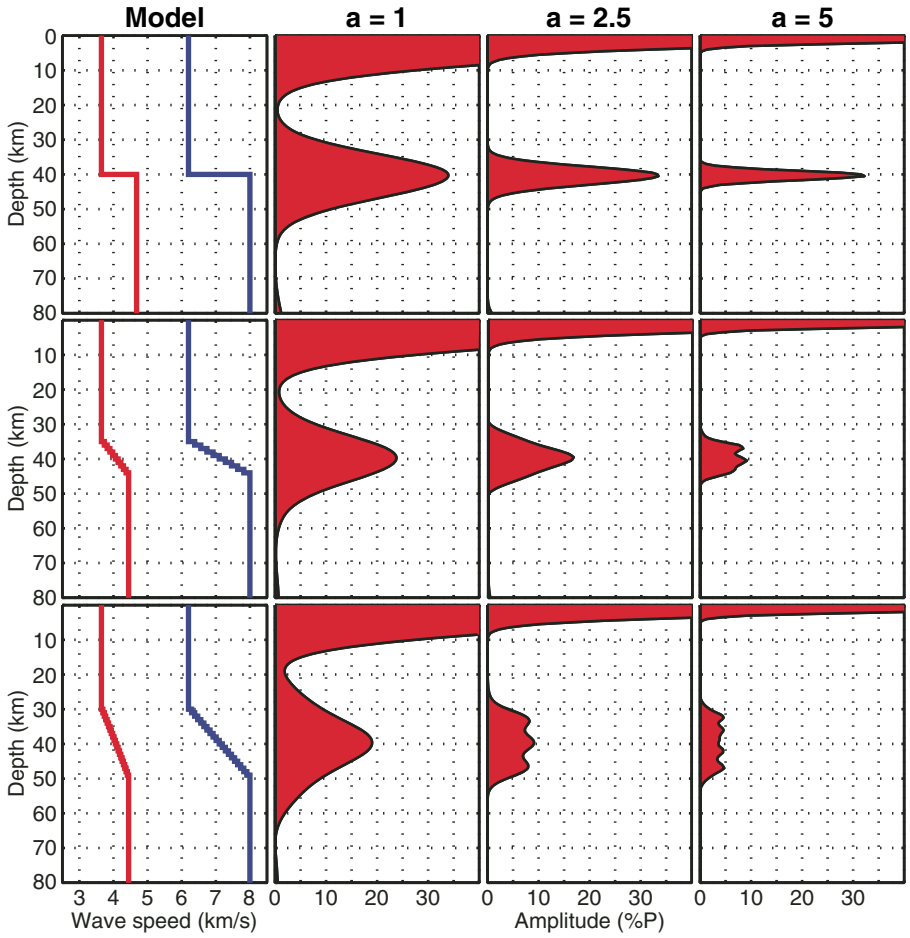

Figure 16. The modeled response of receiver functions to varying *a*-values and gradients for the transition between (6.2/3.65 km/s) crust to (8.0/4.44 km/s) mantle, centered at 40 km depth.

Postsubduction Tectonic Scenarios and the Isabella Anomaly

Our observations further the debate over the end-stage Farallon slab and source of the Isabella anomaly. The opposing tectonic models provide very different outcomes for the fate of the subducted oceanic lithosphere. The slab-window model (Dickinson and Snyder, 1979) entails a scenario where the southern edge of the Farallon–Juan de Fuca plate moves northward and allows asthenosphere to take its place. Consequently the Isabella anomaly stems from the eventual nucleation and detachment of negatively buoyant continental lithosphere (e.g., Zandt, 2003). The stalled slab model (Bohannon and Parsons, 1995) advocates an alternative event, during which portions of the Farallon slab stagnate at the base of the continent beneath California. In this case, the Isabella anomaly represents unsubducted Farallon plate (e.g., Forsyth and Rau, 2009). Regionally low heat-flow extending along the Great Valley, Foothills Metamorphic Belt, and western batholith may result from thermal insulation provided by subcreted oceanic lithosphere (Erkan and Blackwell, 2008) or chilled arclogite (Ducea and Saleeby, 1996), and it is used to model the paleodepth of the subducted plate surface (Erkan and Blackwell, 2009) at 50–70 km beneath the Sierra Nevada. Erkan and Blackwell (2008, 2009) attribute the recent volcanism and uplift along the eastern Sierra Nevada to lateral heat transfer from the Basin and Range to the Great Valley.

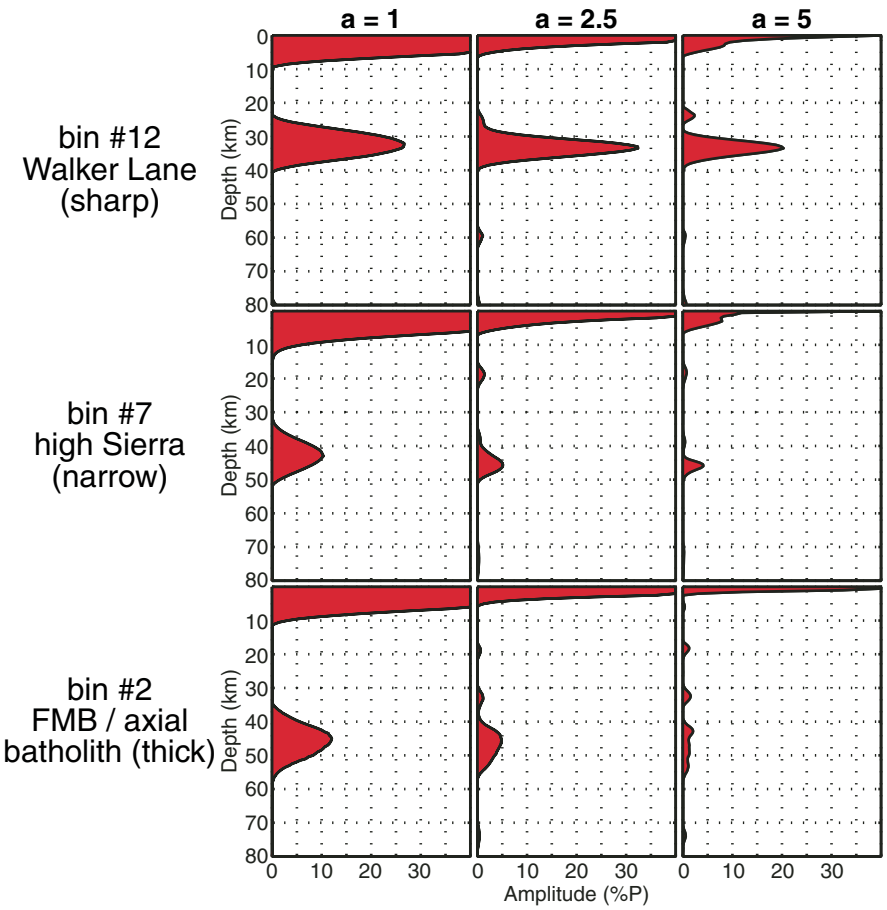

Figure 17. Bins from common–conversion-point stacks along transect K–K′. Different *a*-values illustrate the increasing width of the wave speed contrast along the Moho from east to west.

The stalled slab hypothesis applied to the Sierra Nevada requires scrutiny because it fails to account for known batholithic residue which extended to 100–120 km depth beneath the central Sierra Nevada at ~10 Ma (Ducea and Saleeby, 1998a). This arclogitic lithosphere must have remained intact to be entrained as xenoliths, requiring a regionally deeper Farallon slab. The geometry of subduction appears complicated during the late Mesozoic but favors a deep flat slab beneath the central and northern Sierra Nevada (Saleeby, 2003), similar in geometry to modern flat slabs in South America. Thus models by Erkan and Blackwell (2008) can only validate a slab which deepens significantly approaching the western edge of the batholith, a conclusion advocated by the corresponding interpretation of regional seismic tomography (Forsyth and Rau, 2009).

We directly sample the eastern perimeter of the Isabella anomaly and the shallower fast anomalies along the western batholith resolved by regional tomography (Gilbert et al., 2008; Schmandt and Humphreys, 2010), which is the area where the lingering Farallon slab is suggested to reside (Forsyth and Rau, 2009). Low-frequency receiver functions clearly resolve the conversion from the Moho deepening to >50 km within and/or above the features being interpreted from tomography. The Moho nearest the surface projection of the Isabella anomaly is particularly diffuse. Based on our analysis this weak Moho conversion is clearly produced by a gradient in seismic wave speeds, and it does not appear to be a particularly well-defined structural boundary as could be expected at the boundary of shallow slab. The residue sampled by xenoliths records relatively cool temperatures of 550–950 °C (Ducea and Saleeby, 1996) beneath the batholith. Our observations suggest that the low heat flow inferred to result from a stalled slab results

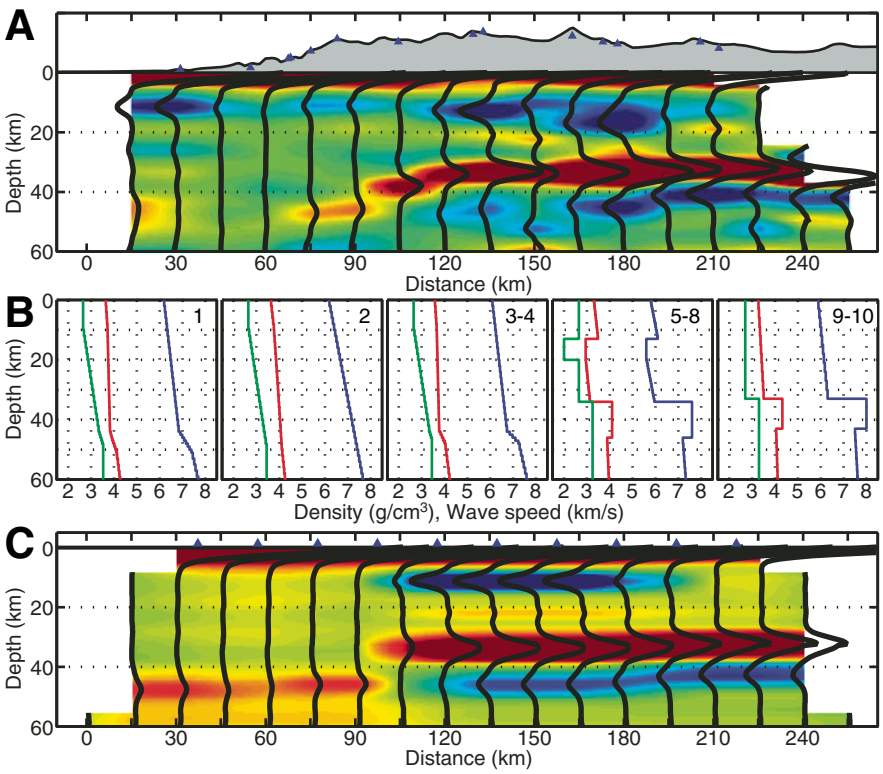

Figure 18. Forward-modeled version of transect K–K′ for *a* = 2.5 receiver functions. A—observed common–conversion-point (CCP) transect, B—models for corresponding station number, C—modeled CCP transect. Displayed model parameters are density (green), Vs (red), and Vp (blue).

instead from the insulation provided by a thick arclogitic root, which is also consistent with the dim Moho arrivals and high wave-speed region identified in tomography.

Summarized Interpretations

We divide the Moho beneath the Sierra Nevada and vicinity into four sections based on its depth (Fig. 9), amplitude (Fig. 10), relation to surface geology, and other constraints (Fig. 19). Much of the east-central and southern Sierra Nevada features a Moho developed after the foundering of its underlying lithospheric mantle during the past few million years. Its sharp amplitude denotes a rapid step in wave speed with depth. Numerous bright spots in the crust and upper mantle appear in conjunction with this delamination Moho (Fig. 20) and provide further evidence of shallow asthenosphere as a source for the volcanism observed in these areas. This region encompasses the locations of Pliocene- and Quaternary-age xenoliths erupted in the eastern Sierra Nevada and high heat-flow measurements. Buoyant uppermost mantle provides the necessary support for the high Sierra Nevada (e.g., Ducea and Saleeby, 1996).

To the west only low-frequency receiver functions exhibit a deeper, less distinct, westward-dipping Moho beneath the west-central Sierra Nevada. This zone represents the gradual transition from relatively light near-surface granitoids through increasingly mafic granulites to dense and eclogitized garnet-clinopyroxenite. We view this as a petrologic Moho (Fig. 19) coincident with the location of intact residue. Several measurements of low heat flow locate near or within this region. The boundary between petrologic and delamination Moho southwest of Yosemite National Park lies adjacent to juxtaposed localities of older arclogite-bearing xenoliths and younger xenoliths that record the invasion of asthenosphere. This suggests that foundering stalled in its westward progression across the south-central Sierra Nevada (Fig. 19). The southward extent of the petrologic Moho forms a salient within delaminated crust and appears to have resisted foundering (Fig. 12 [I–I′]).

Moving northward along the front of the western foothills, receiver functions show intracrustal structure above the petrologic Moho. These structures gradually transition into a discrete, somewhat ragged conversion beneath much of the northern foothills. To the east and north, a somewhat brighter and more coherent Moho appears initially offset from this foothills Moho. We interpret this as a Tertiary or younger tectonic Moho, which underlies much of the northern Sierra Nevada and a portion of the northern and southern Walker Lane. Its amplitude remains lower than the delamination Moho, but higher than the petrologic Moho. We infer that its brightness stems not from sharpening due to the removal of lithospheric mantle, but rather from sustained tectonic reworking due to encroachment of the Basin and Range extension and ongoing magmatic processes such as the episode of dike injection associated with the Lake Tahoe earthquake swarm (Smith et al., 2004). An alternative explanation is that this region underwent an earlier episode of foundering not manifested in presently recognized patterns of volcanism or xenoliths. Future studies of the batholith in this region are necessary to establish if this portion of the batholith did develop a significant residue.

Our final interpretation for ongoing lithospheric removal focuses on the central Sierra Nevada. Gravitationally unstable arclogite founders westward beneath the batholith at 37°–38° N (Fig. 20 [K–K′]). The Moho throughout the eastern Sierra Nevada and western Walker Lane has been reworked due to the recent removal of its underlying lithospheric mantle and ongoing interaction with upwelling asthenosphere. The upwelling produces partial melt that penetrates into the thinned overlying lithosphere. Moving westward, the abrupt change in character of the Moho over ~15 km indicates a rapid transition to thick batholithic residue in the lower crust and upper mantle beneath the axial Sierra Nevada batholith.

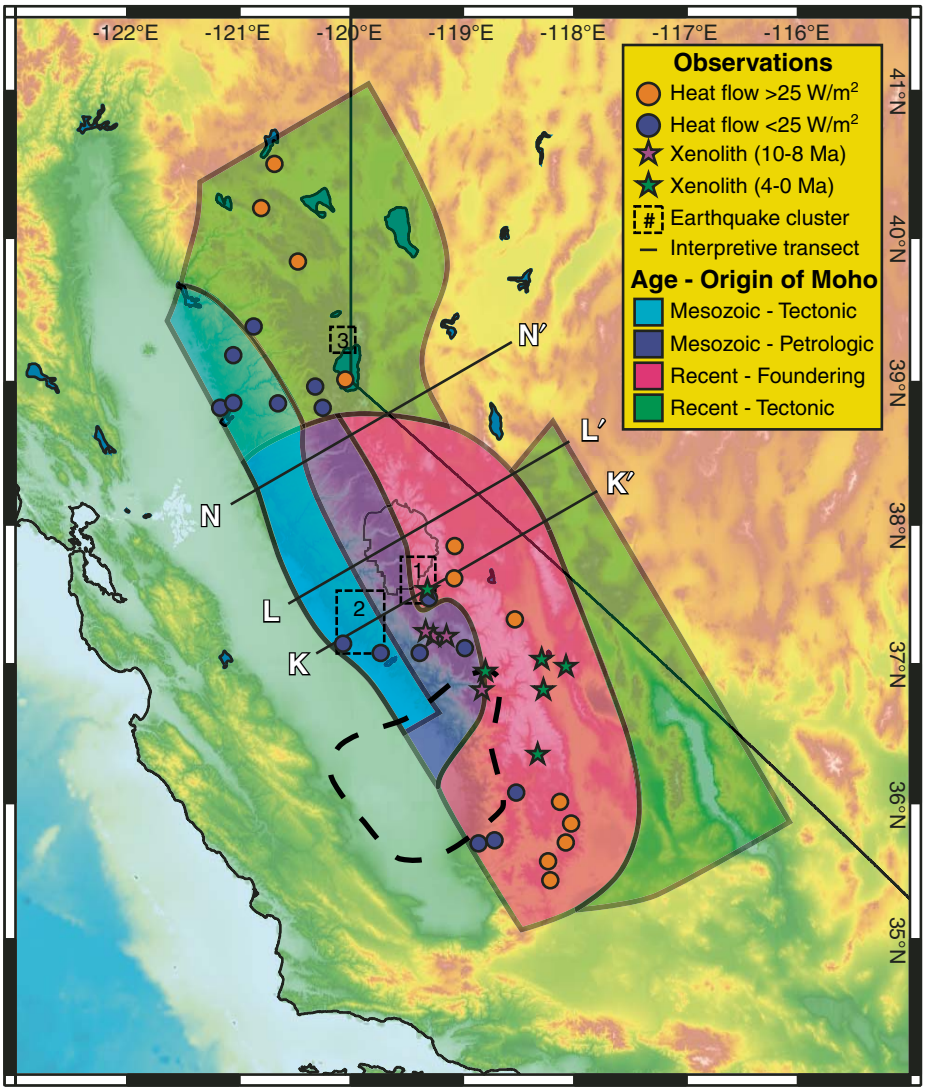

Figure 19. Summary of differing types of Moho observed across the Sierra Nevada with clusters of local seismicity (Hurd et al., 2006; von Seggern et al., 2008), reduced heat-flow measurements (Saltus and Lachenbruch, 1991), and localities of xenoliths (Ducea and Saleeby, 1996, 1998c).

Earthquakes along this transect capture different stages of the foundering process. Along the Great Valley, a zone of seismicity (e.g., Hurd et al., 2006) directly overlies the area where the petrologic Moho occurs over a large depth interval and relates to an initial stage of detachment. We suggest that along the western perimeter of the delamination Moho, long-period earthquakes mark the wedging process where basaltic melts intrude into the lower crust or a low viscosity channel that is actively propagating along the Moho in response to foundering (cf. Le Pourhiet et al., 2006). Decompression melting of rising asthenosphere and subsequent intrusion of melts provides a potential mechanism for triggering these earthquakes. The overlying swarm of crustal seismicity, located as a pipe-like feature (Hurd et al., 2006), may relate to subsequent fluid movement. Farther eastward, inflowing asthenosphere provides a source of magmas for the Long Valley caldera. Whereas both large-scale volcanism and seismicity exist along this corridor, the petrologic Moho and inferred residue persists northward (Fig. 20 [L–L′ and N–N′]). This zone appears to be in an earlier stage of removal. With the northward migration of the slab edge, foundering may proceed roughly from south to north. In the case of the north-central batholith (N–N′), the residue remains relatively undisturbed beneath the central axis of the batholith, coinciding with a general reduction in elevation of the range.

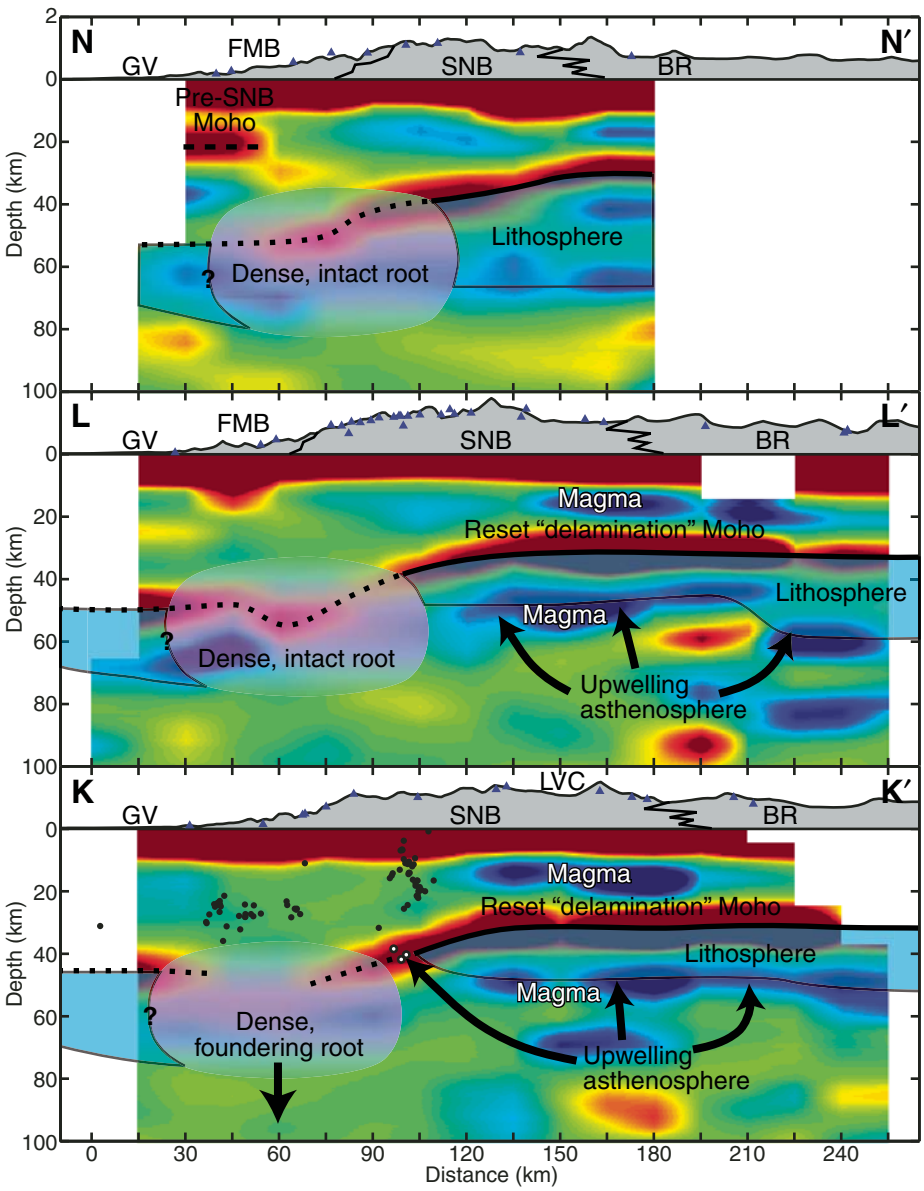

Figure 20. Interpretation of a = 1 receiver-function transects in the central Sierra Nevada. GV—Great Valley, FMB—Foothills Metamorphic Belt, SNB—Sierra Nevada Batholith, LVC—Long Valley caldera, BR—Basin and Range. Transects are marked on Figure 19.

CONCLUSIONS

Phase-weighted, CCP stacks of high-quality teleseismic receiver functions produce an extensive set of observations related to the structure and properties of the crust and upper mantle across the Sierra Nevada and vicinity. The dense data set assembled with the Sierra Nevada EarthScope Project provides new evidence for the presence and ongoing removal of gravitationally unstable, mafic-ultramafic residue. Our data demonstrate that Vp/Vs estimates from CCP stacking may provide more robust and reliable estimates than those produced automatically for individual stations. These measurements show generally lower Vp/Vs across the Sierra Nevada, with pockets of higher Vp/Vs coinciding with recent volcanic centers in the eastern Sierra Nevada and outcrops of ultramafic rocks in the northern Sierra Nevada. Receiver functions sampling the mafic lower crust beneath the western Sierra Nevada batholith allow study of the frequency dependence of the Ps conversion generated by gradational Moho. Subsequent receiver-function modeling demonstrates the importance of considering several frequency ranges to map structure.

The weak Moho presented here represents batholithic residue generated in the late Cretaceous that lingers beneath the central Sierra Nevada. Whereas a wide variety of evidence shows that the southern Sierra Nevada completed its delamination recently, removal of mantle lithosphere beneath the central Sierra Nevada appears to be progressing generally from east to west and south to north, contributing to both deep crustal seismicity and localized volcanism within and along the boundaries of the central Sierra Nevada. Observations from the northern Sierra Nevada show a different structure from the central and southern Sierra Nevada and suggest that the Mesozoic-age batholith may not have produced the dense, garnet-rich residue observed to the south. The continued presence of relatively cool, mafic-ultramafic lithosphere here fits with geologic constraints related to the formation of the Sierra Nevada batholith and provides new insight into the process of lithospheric foundering.

ACKNOWLEDGMENTS

The authors appreciate the thoughtful reviews provided by an anonymous reviewer, Gene Humphreys, and Associate Editor Jason Saleeby. We thank all

involved in SNEP's field program, especially the private landowners and public officials who allowed us access to their land. Standing Order for Data (Owens et al., 2004) and Seismogram Transfer Program were used to collect data for this study. We used code written by Josh Calkins, Generic Mapping Tools (GMT) (Wessel and Smith, 1991) and the m_map package maintained by Rich Pawlowicz. The facilities of the Incorporated Research Institutions for Seismology (IRIS) Data Management System (DMS), and specifically the IRIS Data Management Center, were used for access to waveform and metadata required in this study. Data from the TA network were made freely available as part of the EarthScope USArray facility supported by the National Science Foundation, Major Research Facility program under Cooperative Agreement EAR-0350030. Global Seismographic Network (GSN) is a cooperative scientific facility operated jointly by the IRIS, the U.S. Geological Survey (USGS), and the National Science Foundation (NSF). The IRIS DMS is funded through the National Science Foundation and specifically the GEO Directorate through the Instrumentation and Facilities Program of the National Science Foundation under Cooperative Agreement EAR-0552316. This work was supported by the NSF's EarthScope grants EAR-0454554, EAR-0454524, and EAR-0454535 to the Universities of Arizona, Colorado, and South Carolina. This work was also made possible by funding from the NSF through the Graduate Research Fellowship Program. The lead author gives thanks Barry Reno for a thorough final review and gives a hearty *foghorn* to his friends and family who tolerated many mentions of the Sierra Nevada in otherwise normal conversation.

REFERENCES CITED

Ammon, C.J., Randall, G.E., and Zandt, G., 1990, On the nonuniqueness of receiver function inversions: Journal of Geophysical Research, v. 95, p. 15,303–15,318, doi: 10.1029/JB095iB10p15303.

Anderson, D.L., 2005, Large igneous provinces, delamination, and fertile mantle: Elements, v. 1, p. 271–275, doi: 10.2113/gselements.1.5.271.

Armstrong, R.L., Taubeneck, W.H., and Hales, P.O., 1977, Rb-Sr and K-Ar geochronometry of Mesozoic granitic rocks and their Sr isotopic composition: Oregon, Washington, and Idaho: Geological Society of America Bulletin, v. 88, p. 397–411, doi: 10.1130/0016-7606(1977)88<397:RAKGOM>2.0.CO;2.

Atwater, T., and Stock, J., 1998, Pacific-North America plate tectonics of the Neogene southwestern United States: An update: International Geology Review, v. 40, p. 375–402, doi: 10.1080/00206819809465216.

Barton, M.D., and Hanson, R.B., 1989, Magmatism and the development of low-pressure metamorphic belts: Implications from the western United States and thermal modeling: Geological Society of America Bulletin, v. 101, p. 1051–1065, doi: 10.1130/0016-7606(1989)101<1051:MATDOL>2.3.CO;2.

Bateman, P.C., 1988, Constitution and genesis of the central Sierra Nevada batholith, California: U.S. Geological Survey Open-File Report 88-382, 284 p.

Bateman, P.C., and Eaton, J.P., 1967, Sierra Nevada Batholith: Science, v. 158, p. 1407–1417, doi: 10.1126/science.158.3807.1407.

Benz, H.M., and Zandt, G., 1993, Teleseismic tomography, lithospheric structure of the San Andreas fault system in northern and central California, *in* Iyer, H.M., and Hirahara, K., eds., Seismic Tomography: Theory and Practice: New York, Chapman and Hall, p. 440–465.

Blackwell, D.D., and Richards, M.C., 2004, Geothermal map of North America: American Association of Petroleum Geologists, scale 1:6,500,000.

Bohannon, R.G., and Parsons, T., 1995, Tectonic implications of post–30 Ma Pacific and North American relative plate motions: Geological Society of America Bulletin, v. 107, p. 937–959, doi: 10.1130/0016-7606(1995)107<0937:TIOPMP>2.3.CO;2.

Boyd, O.S., Jones, C.H., and Sheehan, A.F., 2004, Foundering lithosphere imaged beneath the southern Sierra Nevada, California, USA: Science, v. 305, p. 660–662, doi: 10.1126/science.1099181.

Busby, C.J., and Putirka, K., 2009, Miocene evolution of the western edge of the Nevada plano in the central and northern Sierra Nevada: Paleocanyons, magmatism, and structure: International Geology Review, v. 51, p. 670–701, doi: 10.1080/00206810902978265.

Busby, C.J., DeOreo, S.B., Skilling, I., Gans, P.B., and Hagan, J.C., 2008, Carson Pass–Kirkwood paleocanyon system: Paleogeography of the ancestral Cascades arc and implications for landscape evolution of the Sierra Nevada (California): Geological Society of America Bulletin, v. 120, p. 274–299, doi: 10.1130/B25849.1.

Calkins, J.A., Zandt, G., Gilbert, H.J., and Beck, S.L., 2006, Crustal images from San Juan Argentina, obtained using high frequency local event receiver functions: Geophysical Research Letters, v. 33, p. L07309, doi: 10.1029/2005GL025516.

Calkins, J.A., Zandt, G., Girardi, J., Dueker, K., Gehrels, G.E., and Ducea, M.N., 2010, Characterization of the crust of the Coast Mountains Batholith, British Columbia, from P to S converted seismic waves and petrologic modeling: Earth and Planetary Science Letters, v. 289, p. 145–155, doi: 10.1016/j.epsl.2009.10.037.

Cassel, E.L., Graham, S.A., and Chamberlain, C.P., 2009, Cenozoic tectonic and topographic evolution of the northern Sierra Nevada, California, through stable isotope paleoaltimetry in volcanic glass: Geology, v. 37, p. 547–550, doi: 10.1130/G25572A.1.

Cassidy, J.F., 1992, Numerical experiments in borad-band receiver function-analysis: Bulletin of the Seismological Society of America, v. 82, p. 1453–1474.

Chapman, A.D., Kidder, S., Saleeby, J.B., and Ducea, M.N., 2010, Role of extension of the Rand and Sierra de Salinas schists in Late Cretaceous extension and rotation of the southern Sierra Nevada and vicinity: Tectonics, v. 29, p. TC5006, doi: 10.1029/2009TC002597.

Christensen, M.N., 1966, Late Cenozoic crustal movements in the Sierra Nevada of California: Geological Society of America Bulletin, v. 77, p. 163–181, doi: 10.1130/0016-7606(1966)77[163:LCCMIT]2.0.CO;2.

Christensen, N.I., 1996, Poisson's ratio and crustal seismology: Journal of Geophysical Research, v. 101, p. 3139–3156, doi: 10.1029/95JB03446.

Colgan, J.P., Dumitru, T.A., McWilliams, M., and Miller, E.L., 2006a, Timing of Cenozoic volcanism and Basin and Range extension in northwestern Nevada: New constraints from the northern Pine Forest Range: Geological Society of America Bulletin, v. 118, p. 126–139, doi: 10.1130/B25681.1.

Colgan, J.P., Dumitru, T.A., Reiners, P.W., Wooden, J.L., and Miller, E.L., 2006b, Cenozoic tectonic evolution of the Basin and Range province in northwestern Nevada: American Journal of Science, v. 306, p. 616–654, doi: 10.2475/08.2006.02.

Cousens, B., Prytulak, J., Henry, C., Alcazar, A., and Brownrigg, T., 2008, Geology, geochronology, and geochemistry of the Miocene–Pliocene Ancestral Cascades arc, northern Sierra Nevada, California and Nevada: The roles of the upper mantle, subducting slab, and the Sierra Nevada lithosphere: Geosphere, v. 4, p. 829–853, doi: 10.1130/GES00166.1.

Crotwell, H.P., and Owens, T.J., 2005, Automated receiver function processing: Seismological Research Letters, v. 76, p. 702–709, doi: 10.1785/gssrl.76.6.702.

DeCelles, P.G., Ducea, M.N., Kapp, P., and Zandt, G., 2009, Cyclicity in Cordilleran orogenic systems: Nature Geoscience, doi:10.1038/ngeo469.

de Voogd, B., Serpa, L., Brown, L., Hauser, E., Kaufman, S., Oliver, J., Troxel, B.W., Willemin, J., and Wright, L.A., 1986, Death Valley bright spot: A midcrustal magma body in the southern Great Basin, California?: Geology, v. 14, p. 64–67, doi: 10.1130/0091-7613(1986)14<64:DVBSAM>2.0.CO;2.

Dickinson, W.R., 1979, Cenozoic plate tectonic setting of the Cordilleran region in the United States, *in* Armentrout, J.M., Cole, M.R., and TerBest, H., eds., Cenozoic paleogeography of the western United States, *in* Proceedings, Third Pacific Coast Paleogeography Symposium: Los Angeles, Pacific Section, Society of Economic Paleontologists and Mineralogists, p. 1–13.

Dickinson, W.R., 1981, Plate tectonics and the continental margin of California, *in* Ernest, W.G., eds., The Geotectonic Development of California: Englewood Cliffs, New Jersey, Prentice-Hall, p. 1–28.

Dickinson, W.R., 2008, Accretionary Mesozoic–Cenozoic expansion of the Cordilleran continental margin in California and adjacent Oregon: Geosphere, v. 4, p. 329–353, doi: 10.1130/GES00105.1.

Dickinson, W.R., and Snyder, W.S., 1979, Geometry of triple junctions related to San Andreas transform: Journal of Geophysical Research, v. 84, p. 561–572, doi: 10.1029/JB084iB02p00561.

Ducea, M.N., 2001, The California arc: Thick granitic batholiths, eclogitic residues, lithospheric-scale thrusting, and magmatic flare-ups: GSA Today, v. 11, p. 4–10, doi: 10.1130/1052-5173(2001)011<0004:TCATGB>2.0.CO;2.

Ducea, M.N., 2002, Constraints on the bulk composition and root foundering rates of continental arcs: A California arc perspective: Journal of Geophysical Research, v. 107, p. 2304, doi: 10.1029/2001JB000643.

Ducea, M.N., and Saleeby, J.B., 1996, Buoyancy sources for a large, unrooted mountain range, the Sierra Nevada, California: Evidence from xenoliths thermobarometry: Journal of Geophysical Research, v. 101, p. 8229–8244, doi: 10.1029/95JB03452.

Ducea, M.N., and Saleeby, J.B., 1998a, The age and origin of a thick mafic-ultramafic keel from beneath the Sierra Nevada batholiths: Contributions to Mineralogy and Petrology, v. 133, p. 169–185, doi: 10.1007/s004100050445.

Ducea, M.N., and Saleeby, J.B., 1998b, A case for delamination of the deep batholithic crust beneath the Sierra Nevada, California: International Geology Review, v. 40, p. 78–93, doi: 10.1080/00206819809465199.

Ducea, M.N., and Saleeby, J.B., 1998c, Crustal recycling beneath continental arcs: Silica-rich glass inclusions in ultramafic xenoliths from the Sierra Nevada, California, v. 156, p. 101–116.

Dueker, K.G., and Sheehan, A.F., 1997, Mantle discontinuity structure from midpoint stacks of converted P to S waves across the Yellowstone hotspot track: Journal of Geophysical Research, v. 102, p. 8313–8327, doi: 10.1029/96JB03857.

Dueker, K.G., and Sheehan, A.F., 1998, Mantle discontinuity structure beneath the Colorado Rocky Mountains and High Plains: Journal of Geophysical Research, v. 103, p. 7153–7169, doi: 10.1029/97JB03509.

Efron, B., and Tibshirani, R., 1986, Bootstrap methods for standard errors, confidence intervals, and other measures of statistical accuracy: Statistical Science, v. 1, p. 54–77, doi: 10.1214/ss/1177013815.

Erkan, K., and Blackwell, D.D., 2008, A thermal test of the post-subduction tectonic evolution along the California transform margin: Geophysical Research Letters, v. 35, p. L07309, doi: 10.1029/2008GL033479.

Erkan, K., and Blackwell, D.D., 2009, Transient thermal regimes in the Sierra Nevada and Baja California extinct outer arcs following the cessation of Farallon subduction: Journal of Geophysical Research, v. 114, p. B02107, doi: 10.1029/2007JB005498.

Farmer, G.L., Glazner, A.F., and Manley, C.R., 2002, Did lithospheric delamination trigger late Cenozoic potassic volcanism in the Sierra Nevada, California?: Geological Society of America Bulletin, v. 114, p. 754–768, doi: 10.1130/0016-7606(2002)114<0754:DLDTLC>2.0.CO;2.

Fliedner, M.M., Ruppert, S.D., Malin, P.E., Park, S.K., Jiracek, G.R., Phinney, R.A., Saleeby, J.B., Wernicke, B.P., Clayton, R.W., Keller, G.R., Miller, K.C., Jones, C.H., Luetgert, J.H., Mooney, W.D., Oliver, H.L., Klemperer, S.L., and Thompson, G.A., 1996, Three-dimensional crustal structure of the southern Sierra Nevada from seismic fan profiles and gravity modeling: Geology, v. 24, p. 367–370, doi: 10.1130/0091-7613(1996)024<0367:TDCSOT>2.3.CO;2.

Fliedner, M.M., Klemperer, S.L., and Christensen, N.I., 2000, Three-dimensional seismic model of the Sierra Nevada arc, California, and its implications

for crustal and upper mantle composition: Journal of Geophysical Research, v. 105, p. 10,899–10,921, doi: 10.1029/2000JB900029.

Forsyth, D.W., and Rau, C.J., 2009, Isabella anomaly: Lithospheric drip, delamination or fragment of the Farallon plate: Eos (Transactions, American Geophysical Union), v. 90, no. 52.

Frassetto, A., Zandt, G., Gilbert, H., Owens, T.J., and Jones, C.H., 2010, Improved imaging with phase-weighted common conversion point stacks of receiver functions: Geophysical Journal International, doi: 10.1111/j.1365-246X.2010.04617.x.

Gilbert, H.J., and Sheehan, A.F., 2004, Images of crustal variations in the intermountain west: Journal of Geophysical Research, v. 109, p. B03306, doi: 10.1029/2003JB002730.

Gilbert, H.J., Sheehan, A.F., Dueker, K.G., and Molnar, P., 2003, Receiver functions in the western United States, with implications for upper mantle structure and dynamics: Journal of Geophysical Research, v. 108, p. 2229, doi: 10.1029/2001JB001194.

Gilbert, H., Jones, C., Owens, T.J., and Zandt, G., 2007, Imaging Sierra Nevada Lithospheric Sinking: Eos (Transactions, American Geophysical Union), v. 88, no. 21, p. 225, doi: 10.1029/2007EO210001.

Gilbert, H., Yang, Y., Forsyth, D.W., Jones, C.H., Owens, T.J., and Zandt, G., 2008, Bounds of foundering in the southern Sierra Nevada: Eos (Transactions, American Geophysical Union), v. 89, no. 53.

Gurrola, H., Minster, J.B., and Owens, T., 1994, The use of velocity spectrum for stacking receiver functions and imaging upper mantle discontinuities: Geophysical Journal International, v. 117, p. 427–440, doi: 10.1111/j.1365-246X.1994.tb03942.x.

Hacker, B.R., and Abers, G.A., 2004, Subduction factory: 3. An Excel worksheet and macro for calculating the densities, seismic wave speeds, and H_2O contents of minerals and rocks at pressure and temperature: Geochemistry Geophysics Geosystems, v. 5, p. Q01005, doi: 10.1029/2003GC000614.

Harwood, D.S., and Helley, E.J., 1987, Late Cenozoic Tectonism of the Sacramento Valley, California: U.S. Geological Survey Professional Paper 1359, 46 p.

Hayes, G.P., and Furlong, K.P., 2007, Abrupt changes in crustal structure beneath the Coast Ranges of northern California—Developing new techniques in receiver function analysis: Geophysical Journal International, v. 170, p. 313–336, doi: 10.1111/j.1365-246X.2007.03401.x.

Heimgartner, M., Louie, J.N., Scott, J.B., Thelen, W., Lopez, C.T., and Coolbaugh, M., 2006, The crustal thickness of the Great Basin: Using seismic refraction to assess regional geothermal potential: Geothermal Resources Council Transactions, v. 30, p. 81–86.

Huber, N.K., 1981, Amount and timing of late Cenozoic uplift and tilt of the central Sierra Nevada, California—Evidence from the upper San Joaquin River basin: U.S. Geological Survey Paper 1197, 28 p.

Hurd, O., Frassetto, A., Zandt, G., Gilbert, H., Jones, C., and Owens, T.J., 2006, Deep crustal earthquakes and repeating earthquakes in the west-central Sierra Nevada, western USA: Eos (Transactions, American Geophysical Union), v. 87, no. 52.

Jones, C.H., 1987, Is extension in Death Valley accommodated by thinning of the mantle lithosphere beneath the Sierra Nevada, California?: Tectonics, v. 6, p. 449–473, doi: 10.1029/TC006i004p00449.

Jones, C.H., and Phinney, R.A., 1998, Seismic structure of the lithosphere from teleseismic converted arrivals observed at small arrays in the southern Sierra Nevada and vicinity, California: Journal of Geophysical Research, v. 103, p. 10,065–10,090, doi: 10.1029/97JB03540.

Jones, C.H., Kanamori, H., and Roecker, S.W., 1994, Missing roots and mantle "drips": Regional Pn and teleseismic arrival times in the southern Sierra Nevada and vicinity, California: Journal of Geophysical Research, v. 99, p. 4567–4601, doi: 10.1029/93JB01232.

Jones, C.H., Farmer, G.L., and Unruh, J., 2004, Tectonics of Pliocene removal of lithosphere of the Sierra Nevada, California: Geological Society of America Bulletin, v. 116, p. 1408–1422, doi: 10.1130/B25397.1.

Jones, L.M., and Dollar, R.S., 1986, Evidence of Basin-and-Range extensional tectonics in the Sierra Nevada: The Durrwood Meadows swarm, Tulare County, California (1983–1984): Bulletin of the Seismological Society of America, v. 76, p. 439–461.

Julià, J., 2007, Constraining velocity and density contrasts across the crust-mantle boundary with receiver function amplitudes: Geophysical Journal International, v. 171, p. 286–301, doi: 10.1111/j.1365-2966.2007.03502.x.

Kay, R.W., and Kay, S.M., 1991, Creation and destruction of lower continental crust: Geologische Rundschau, v. 80, p. 259–278, doi: 10.1007/BF01829365.

Keir, D., Bastow, I.D., Whaler, K.A., Daly, E., Cornwell, D.G., and Hautot, S., 2009, Lower crustal earthquakes near the Ethiopian rift induced by magmatic processes: Geochemistry Geophysics Geosystems, v. 10, Q0AB02, doi:10.1029/2009GC002382.

Kelemen, P.B., Hanghoj, K., and Greene, A.R., 2003, One view of the geochemistry of subduction-related magmatic arcs, with an emphasis on primitive andesites and lower crust, *in* Rudnick, R.L., ed., The Crust, Volume 3; *in* Holland, H.D., and Turekian, K.K., eds., Treatise on Geochemistry: Oxford, Elsevier-Pergamon, p. 593–659.

Kennett, B.L.N., and Engdahl, E.R., 1991, Traveltimes for global earthquake location and phase identification: Geophysical Journal International, v. 105, p. 429–465.

Klein, C., and Hurlbut, C.S., Jr. (after Dana, J.D.), 1999, Manual of Mineralogy: New York, John Wiley and Sons, Inc., 681 p.

Lachenbruch, A.H., and Sass, J.H., 1977, Heat flow in the United States and the thermal regime of the crust, *in* Heacock, J.G., ed., The Earth's Crust, Its Nature and Physical Properties: Washington, D.C., American Geophysical Union, p. 626–675.

Langston, C.A., 1979, Structure under Mount Rainier, Washington, inferred from teleseismic body waves: Journal of Geophysical Research, v. 84, p. 4749–4762, doi: 10.1029/JB084iB09p04749.

Le Pourhiet, L., Gurnis, M., and Saleeby, J., 2006, Mantle instability beneath the Sierra Nevada Mountains in California and Death Valley extension: Earth and Planetary Science Letters, v. 251, p. 104–119, doi: 10.1016/j.epsl.2006.08.028.

Li, X., Yuan, X., and Kind, R., 2007, The lithosphere-asthenosphere boundary beneath the western United States: Geophysical Journal International, v. 170, p. 700–710, doi: 10.1111/j.1365-246X.2007.03428.x.

Ligorría, J., and Ammon, C.J., 1999, Iterative deconvolution of teleseismic seismograms and receiver function estimation: Bulletin of the Seismological Society of America, v. 89, p. 1395–1400.

Locock, A., 2008, An Excel spreadsheet to recast analyses of garnet into end-member components, and a synopsis of the crystal chemistry of natural silicate garnets: Computers and Geosciences, v. 34, p. 1769–1780.

Lombardi, D., Braunmiller, J., Kissling, E., and Giardini, D., 2008, Moho depth and Poisson's ratio in the Western-Central Alps from receiver functions: Geophysical Journal International, v. 173, p. 249–264, doi: 10.1111/j.1365-246X.2007.03706.x.

Louie, J.N., Thelen, W., Smith, S.B., Scott, J.B., Clark, M., and Pullammanappallil, S., 2004, The northern Walker Lane refraction experiment: Pn arrivals and the northern Sierra Nevada root: Tectonophysics, v. 388, p. 253–269, doi: 10.1016/j.tecto.2004.07.042.

Mahéo, G., Saleeby, J., Saleeby, Z., and Farley, K.A., 2009, Tectonic control on southern Sierra Nevada topography, California: Tectonics, v. 28, p. TC6006, doi: 10.1029/2008TC002340.

Malin, P.E., Goodman, E.D., Henyey, T.L., Li, Y.G., Okaya, D.A., and Saleeby, J.B., 1995, Significance of seismic reflections beneath a tilted exposure of deep continental crust, Tehachapi Mountains, California: Journal of Geophysical Research, v. 100, p. 2069–2087, doi: 10.1029/94JB02127.

Manley, C.R., Glazner, A.F., and Farmer, G.L., 2000, Timing of volcanism in the Sierra Nevada of California: Evidence for the Pliocene delamination of the batholithic root?: Geology, v. 28, p. 811–814, doi: 10.1130/0091-7613(2000)28<811:TOVITS>2.0.CO;2.

May, J.C., and Hewitt, R.L., 1948, The basement complex in well samples from Sacramento and San Joaquin Valleys, California: California Division of Mines and Geology Journal, v. 44, p. 129–158.

Miller, K.C., and Mooney, W.D., 1994, Crustal structure and composition of the southern Foothills Metamorphic Belt, Sierra Nevada, California, from seismic data: Journal of Geophysical Research, v. 99, p. 6865–6880, doi: 10.1029/93JB02755.

Mukhopadhyay, B., and Manton, W.I., 1994, Upper-Mantle fragments from beneath the Sierra Nevada batholith: Partial fusion, fractional crystallization, and metasomatism in a subduction-related ancient lithosphere: Journal of Petrology, v. 35, p. 1417–1450.

Nadin, E.S., and Saleeby, J.B., 2008, Disruption of regional primary structure of the Sierra Nevada batholith by the Kern Canyon fault system, California, *in* Wright, J.E., and Shervais, J.W., eds., Ophiolites, Arcs, and Batholiths: Geological Society of America Special Paper 438, p. 429–453.

Oliver, H.W., 1977, Gravity and magnetic investigations of the Sierra Nevada batholith, California: Geological Society of America Bulletin, v. 88, p. 445–461, doi: 10.1130/0016-7606(1977)88<445:GAMIOT>2.0.CO;2.

Ostos, L., and Park, S.K., 2008, Magnetotelluric transect through Yosemite reveals evidence of Sierran delamination: Eos (Transactions, American Geophysical Union), v. 89, no. 53.

Owens, T.J., and Zandt, G., 1985, The response of the continental crust-mantle boundary observed on broadband teleseismic receiver functions: Geophysical Research Letters, v. 12, p. 705–708, doi: 10.1029/GL012i010p00705.

Owens, T.J., Zandt, G., and Taylor, S.R., 1984, Seismic evidence for an ancient rift beneath the Cumberland plateau, Tennessee: A detailed analysis of broadband teleseismic p waveforms: Journal of Geophysical Research, v. 89, p. 7783–7795, doi: 10.1029/JB089iB09p07783.

Owens, T.J., Crotwell, H.P., Groves, C., and Oliver-Paul, P., 2004, SOD: Standing Order for Data: Seismological Research Letters, v. 75, p. 515–520.

Park, S., 2004, Mantle heterogeneity beneath eastern California from magnetotelluric measurements: Journal of Geophysical Research, v. 109, p. B09406, doi: 10.1029/2003JB002948.

Parrish, J.G., 2006, Simplified Geologic Map of California: California Geological Survey Map Sheet 57.

Pitt, A.M., Hill, D.P., Walter, S.W., and Johnson, M.J.S., 2002, Midcrustal, long-period earthquakes beneath northern California volcanic areas: Seismological Research Letters, v. 73, p. 144–152, doi: 10.1785/gssrl.73.2.144.

Reeg, H., Jones, C.H., Gilbert, H., Owens, T.J., and Zandt, G., 2008, Tomographic observations connecting convective downwellings with lithospheric source regions, Sierra Nevada, California: Eos (Transactions, American Geophysical Union), v. 89, no. 53.

Ruppert, S., Fliedner, M.M., and Zandt, G., 1998, Thin crust and active upper mantle beneath the southern Sierra Nevada in the western United States: Tectonophysics, v. 286, p. 237–252, doi: 10.1016/S0040-1951(97)00268-0.

Saleeby, J., 2003, Segmentation of the Laramide slab —Evidence from the southern Sierra Nevada region: Geological Society of America Bulletin, v. 115, p. 655–668, doi: 10.1130/0016-7606(2003)115<0655:SOTLSF>2.0.CO;2.

Saleeby, J., 2007, The western extent of the Sierra Nevada batholith in the Great Valley basement and its significance in underlying mantle dynamics: Eos (Transactions, American Geophysical Union), v. 88, no. 52.

Saleeby, J., and Foster, Z., 2004, Topographic response to mantle lithosphere removal in the southern Sierra Nevada region, California: Geology, v. 32, p. 245–248, doi: 10.1130/G19958.1.

Saleeby, J., Ducea, M., and Clemens-Knott, D., 2003, Production and loss of high-density batholithic root, southern Sierra Nevada, California: Tectonics, v. 22, doi: 10.1029/2002TC001374.

Saleeby, J., Saleeby, Z., Nadin, E., and Mahéo, G., 2009, Step-over in the structure controlling the regional west tilt of the Sierra Nevada microplate: Eastern escarpment system to Kern Canyon system: International Geology Review, v. 51, p. 634–669, doi: 10.1080/00206810902867773.

Saleeby, J.B., 1990, Geochronologic and tectonostratigraphic framework of Sierra-Klamath ophiolitic

assemblages, *in* Harwood, D.S. and Miller, M.M., eds., Paleozoic and Early Mesozoic Paleogeographic Relations, Sierra Nevada, Klamath Mountains, and Related Terranes: Geological Society of America Special Paper 255, p. 93–114.

Saleeby, J.B., 1992, Petrotectonic and paleogeographic settings of U.S. Cordilleran ophiolites, *in* Burchfiel, B.C., et al., eds., The Cordilleran Orogen: Conterminous U.S.: Boulder, Colorado, Geological Society of America, Geology of North America, v. G-3, p. 653–682.

Saleeby, J.B., Shaw, H.F., Niemeyer, S., Moores, E.M., and Edelman, S.H., 1989, U/Pb, Sm/Nd and Rb/Sr geochronological and isotopic study of northern Sierra Nevada ophiolitic assemblages, California: Contributions to Mineralogy and Petrology, v. 102, p. 205–220, doi: 10.1007/BF00375341.

Saltus, R.W., and Lachenbruch, A.H., 1991, Thermal evolution of the Sierra Nevada: Tectonic implications of new heat flow data: Tectonics, v. 10, p. 325–344, doi: 10.1029/90TC02681.

Savage, B., Ji, C., and Helmberger, D.V., 2003, Velocity variations in the uppermost mantle beneath the southern Sierra Nevada and Walker Lane: Journal of Geophysical Research, v. 108, p. 2325, doi: 10.1029/2001JB001393.

Savage, M.K., Li, L., Eaton, J.P., Jones, C.H., and Brune, J.N., 1994, Earthquake refraction profiles of the root of the Sierra Nevada: Tectonics, v. 13, p. 803–817, doi: 10.1029/93TC03488.

Schimmel, M., and Paulssen, H., 1997, Noise reduction and detection of weak, coherent signals through phase-weighted stacks: Geophysical Journal International, v. 130, p. 497–505, doi: 10.1111/j.1365-246X.1997.tb05664.x.

Schmandt, B., and Humphreys, E., 2010, Seismic heterogeneity and small-scale convection in the southern California upper mantle: Geochemistry Geophysics Geosystems, v. 11, p. Q05004, doi: 10.1029/2010GC003042.

Schweickert, R.A., Bogen, N.L., Girty, G.H., Hanson, R.E., and Merguerian, C., 1984, Timing and structural expression of the Nevadan Orogeny, Sierra Nevada, California: Geological Society of America Bulletin, v. 95, p. 967–979, doi: 10.1130/0016-7606(1984)95<967:TASEOT>2.0.CO;2.

Sheetz, K.E., and Schlue, J.W., 1992, Inferences for the Socorro magma body from teleseismic receiver functions: Geophysical Research Letters, v. 19, p. 1867–1870, doi: 10.1029/92GL02137.

Smith, K.D., von Seggern, D., Blewitt, G., Preston, L., Anderson, J.G., Wernicke, B.P., and Davis, J.L., 2004, Evidence for deep magma Injection beneath Lake Tahoe, Nevada-California: Science, v. 305, p. 1277–1280, doi: 10.1126/science.1101304.

Spieth, M.A., Hill, D.P., and Geller, R.J., 1981, Crustal structure in the northwestern foothills of the Sierra Nevada from seismic refraction experiments: Bulletin of the Seismological Society of America, v. 71, p. 1075–1087.

Thurber, C., Zhang, H., Brocher, T., and Langenheim, V., 2009, Regional three-dimensional seismic velocity model of the crust and uppermost mantle of northern California: Journal of Geophysical Research, v. 114, p. B01304, doi: 10.1029/2008JB005766.

Unruh, J.R., 1991, The uplift of the Sierra Nevada and implications for late Cenozoic epeirogeny in the western Cordillera: Geological Society of America Bulletin, v. 103, p. 1395–1404, doi: 10.1130/0016-7606(1991)103<1395:TUOTSN>2.3.CO;2.

Van Buer, N.J., Miller, E.L., and Dumitru, T.A., 2009, Early Tertiary paleogeologic map of the northern Sierra Nevada batholith and the northwestern Basin and Range: Geology, v. 37, p. 371–374, doi: 10.1130/G25448A.1.

von Seggern, D.H., Smith, K.D., and Preston, L.A., 2008, Seismic spatial-temporal character and effects of a deep (25–30 km) magma intrusion below north Lake Tahoe, California-Nevada: Bulletin of the Seismological Society of America, v. 98, p. 1508–1526, doi: 10.1785/0120060240.

Wadati, K., 1933, On the travel time of earthquake waves, II: Geophysical Magazine, v. 7, p. 101–111.

Wakabayashi, J., and Sawyer, T.L., 2001, Stream incision, tectonics, uplift, and evolution of topography of the Sierra Nevada, California: The Journal of Geology, v. 109, p. 539–562, doi: 10.1086/321962.

Wernicke, B., Clayton, R., Ducea, M., Jones, C.H., Park, S., Ruppert, S., Saleeby, J., Snow, J.K., Squires, L., Fliedner, M., Jiracek, G., Keller, R., Klemperer, S., Luetgert, J., Malin, P., Miller, K., Mooney, W., Oliver, H., and Phinney, R., 1996, Origin of high mountains in the continents: The southern Sierra Nevada: Science, v. 271, p. 190–193, doi: 10.1126/science.271.5246.190.

Wessel, P., and Smith, W.H.F., 1991, Free software helps map and display data: Eos (Transactions, American Geophysical Union), v. 72, p. 441, doi: 10.1029/90EO00319.

Williams, H., and Curtis, G.H., 1977, The Sutter Buttes of California: A Study of Plio-Pleistocene Volcanism: University of California Publications in Geological Sciences, v. 116, 57 p.

Wilson, C.K., Jones, C.H., and Gilbert, H.J., 2003, Single-chamber silicic magma system inferred from shear wave discontinuities of the crust and uppermost mantle, Coso geothermal area, California: Journal of Geophysical Research, v. 108, p. 2226, doi: 10.1029/2002JB001798.

Wolf, M.B., and Saleeby, J.B., 1992, Jurassic Cordilleran dike swarm-shear zones: Implications for the Nevadan orogeny and North American plate motion: Geology, v. 20, p. 745–748, doi: 10.1130/0091-7613(1992)020<0745:JCDSSZ>2.3.CO;2.

Wong, I.G., and Savage, W.U., 1983, Deep intraplate seismicity in the western Sierra Nevada, central California: Bulletin of the Seismological Society of America, v. 73, p. 792–812.

Wood, D.J., and Saleeby, J.B., 1998, Late Cretaceous-Paleocene extensional collapse and disaggregation of the southernmost Sierra Nevada batholith: International Geology Review, v. 39, p. 289–325.

Yan, Z., and Clayton, R.W., 2007, Regional mapping of the crustal structure in southern California from receiver functions: Journal of Geophysical Research, v. 112, p. B05311, doi: 10.1029/2006JB004622.

Yang, Y., and Forsyth, D.W., 2006, Rayleigh wave phase velocities, small-scale convection, and azimuthal anisotropy beneath southern California: Journal of Geophysical Research, v. 111, p. B07306, doi: 10.1029/2005JB004180.

Zandt, G., 2003, The southern Sierra Nevada drip and the mantle wind direction beneath the southwestern United States: International Geology Review, v. 45, p. 213–224, doi: 10.2747/0020-6814.45.3.213.

Zandt, G., and Ammon, C.J., 1995, Continental crust composition constrained by measurements of crustal Poisson's ratio: Nature, v. 374, p. 152–154, doi: 10.1038/374152a0.

Zandt, G., Myers, S.C., and Wallace, T.C., 1995, Crust and mantle structure across the Basin and Range-Colorado Plateau boundary at 37° N latitude and implications for Cenozoic extensional mechanism: Journal of Geophysical Research, v. 100, p. 10,529–10,548, doi: 10.1029/94JB03063.

Zandt, G., Gilbert, H., Owens, T.J., Ducea, M., Saleeby, J., and Jones, C.H., 2004, Active foundering of a continental arc root beneath the southern Sierra Nevada in California: Nature, v. 431, p. 41–46, doi: 10.1038/nature02847.

Zhu, L., and Kanamori, H., 2000, Moho depth variation in southern California from teleseismic receiver functions: Journal of Geophysical Research, v. 105, p. 2969–2980, doi: 10.1029/1999JB900322.

Manuscript Received 30 November 2009
Revised Manuscript Received 15 February 2011
Manuscript Accepted 18 March 2011